Review

Application of NH₃ Fuel in Power Equipment and Its Impact on NOₓ Emissions

Jinyi Hu, Yongbao Liu *,†, Xing He *,†, Jianfeng Zhao and Shaojun Xia

College of Power Engineering, Naval University of Engineering, Wuhan 430033, China;
hujinyi2535@163.com (J.H.); jianfeng62300_zhao@163.com (J.Z.); shaojunxia_2021@163.com (S.X.)
* Correspondence: liuyongbaoly@163.com (Y.L.); hexing_mail@163.com (X.H.); Tel.: +86-27-65460593 (X.H.)
† These authors contributed equally to this work.

Abstract: Due to high greenhouse gas emissions, countries worldwide are stepping up their emission reduction efforts, and the global demand for new, carbon-free fuels is growing. Ammonia (NH_3) fuels are popular due to their high production volume, high energy efficiency, ease of storage and transportation, and increased application in power equipment. However, their physical characteristics (e.g., unstable combustion, slow flame speed, and difficult ignition) limit their use in power equipment. Based on the structural properties of the power equipment, NH_3 fuel application and emissions characteristics were analyzed in detail. Combustion of NH_3 fuels and reduction measures for NO_x emissions (spark plug ignition, compression ignition, and gas turbines) were analyzed from various aspects of operating conditions (e.g., mixed fuel, fuel-to-exhaust ratio, and equivalence ratio), structure and strategy (e.g., number of spark plugs, compression ratio (CR), fuel injection, and ignition mode), and auxiliary combustion techniques (e.g., preheating, humidification, exhaust gas recirculation, and secondary air supply). The performance of various NH_3 fuel cell (FC) types was analyzed, with a focus on the maximum power achievable for different electrolyte systems. Additionally, the application and NO_x emissions of indirect NH_3 FCs were evaluated under flame and catalytic combustion conditions. The system efficiency of providing heat sources by burning pure NH_3, anode tail gas, and NH_3 decomposition gas was also compared. Based on a comprehensive literature review, the key factors influencing the performance and emissions of NH_3-powered equipment were identified. The challenges and limitations of NH_3-powered equipment were summarized, and potential strategies for improving efficiency and reducing emissions were proposed. These findings provide valuable insights for the future development and application of NH_3 FCs.

Keywords: NH_3 fuel; operating conditions; structure and strategy; auxiliary combustion; influence factor threshold; power equipment

1. Introduction

The issue of global warming, which is brought about by the excessive release of greenhouse gases, has become a pressing concern that humans must urgently address [1–3]. Reducing emissions is the primary means of achieving the "two-carbon" goals [4]. Controlling global warming at 1.5 °C instead of 2 °C would bring significant advantages to humanity, encompassing aspects such as sea level rise, meteorological disaster, water scarcity, permafrost thawing, and more [5]. The largest obstacle we face in our generation is climate change. To meet the temperature criterion of 1.5 °C laid down by the Intergovernmental Panel on Climate Change and reduce global greenhouse gas emissions, it is imperative to identify technically reliable, commercially significant, environmentally friendly, and safe solutions [6,7]. The global response to greenhouse gases is shown in Figure 1.
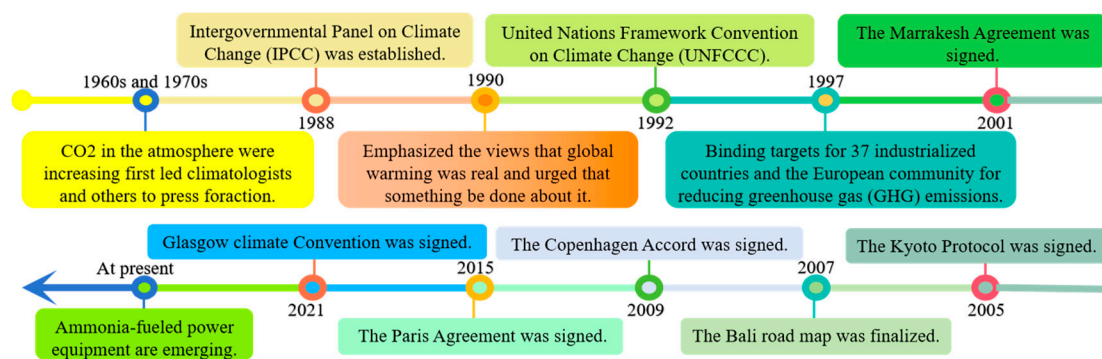
Figure 1. Global action to reduce emissions.

With the pressing need to address climate change, vigorously developing renewable and carbon-free energy sources has become paramount [1–3]. Energy carriers are crucial in balancing intermittent renewable energy production with ever-increasing demand [8,9]. For the mass transportation of hydrogen-containing fuels, liquefied forms of energy storage are preferred [10]. Liquid fuels, including liquid hydrogen or hydrogen-containing carriers such as ammonia (NH_3), have gained traction in various applications [11,12]. Safe, reliable, and easily transportable energy is essential for achieving the "two-carbon" goals [13,14]. However, the lack of large-scale, reliable infrastructure hampers the efficient storage and transportation of hydrogen energy [15,16]. In contrast to hydrogen, NH_3 energy boasts a well-established global infrastructure, a complete industrial chain for production, transportation, storage, and terminal applications, and favorable physical properties such as higher energy density [17]. These advantages position NH_3 as a promising alternative to fossil fuels, with green NH_3 production technologies further enhancing its appeal as a sustainable decarbonization fuel [18–20]. Moreover, NH_3 exhibits superior safety compared to methane (CH_4), hydrogen, liquefied petroleum gas, methanol, and gasoline [17,21]. As evident from Table 1, NH_3 is emerging as a frontrunner for future renewable energy solutions [17,21–23]. Its cost-effectiveness, low carbon emissions, high efficiency, and safety make it a compelling choice to replace carbon-based energy sources. However, as NH_3 energy gains recognition, it is crucial to closely monitor pollutant emissions and the far-reaching impacts of the nitrogen cycle on the global environment throughout NH_3's life cycle, from nitrogen synthesis to final decomposition [24–26]. NH_3 fuel applications and emissions as shown in Figure 2.

Table 1. Physical property parameters of fuel [27].

| Property	NH_3	Gasoline	n-Heptane	Diesel	CH_4	H_2
Lower heating value (MJ/kg)	18.8	44.5	44.6	45	50	120
Density at 1 bar and 298 K (kJ/m^3)	0.72	736	684	849	0.67	0.09
Vaporizing heat (kJ/kg)	1370	348.7	320	232.4	511	455
Autogenous ignition temperature (K)	930	503	477	527–558	859	773–850
Laminar burning velocity (m/s) (close to stoich)	0.07	0.58	0.37	0.86	0.38	3.51
Flammability limit (vol. %)	15–28	0.6–8	1.05–6.7	1–6	5–15	4.7–75
Air/fuel ratio by mass	6.05	15	15.4	14.5	17.3	34.6
Octane number	130	90–98	0	-	120	>100
Adiabatic flame temperature (K)	1800	2138	2294	2300	1950	2110
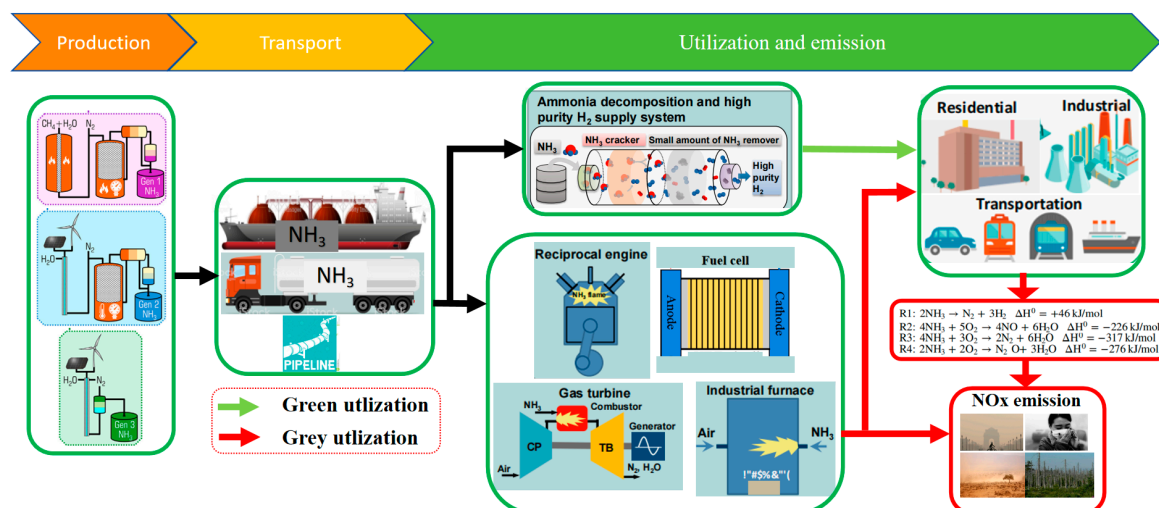
Figure 2. NH$_3$ fuel applications and emissions [21,26].

Utilizing alternative energy sources through minor modifications in carbonaceous energy-powered equipment presents a rapid and cost-effective approach to developing NH$_3$ energy [28]. However, NH$_3$ combustion faces challenges such as ignition difficulties, slow flame propagation, and instability. Additionally, a low heat release rate (HRR) and high NO$_x$ emissions hinder the widespread use of NH$_3$ in power equipment. NH$_3$ also serves as an effective hydrogen carrier, enabling the decomposition of NH$_3$ to generate hydrogen as a green energy source. Simultaneously, NH$_3$ fuel can participate in FC reactions to produce a stream of electrons, generating electricity [8]. However, NH$_3$'s weak reaction kinetics and slow chemical reaction rate limit its power output and hinder its broader application in fuel cells (FCs) [17]. Mixing NH$_3$ with fuels with higher reactivity can effectively improve its combustion rate. Other measures, such as structural adjustments, strategic optimization, and auxiliary combustion technologies, have also yielded promising results in enhancing NH$_3$ combustion [17].

To advance the application of NH$_3$ power equipment, researchers have delved into NH$_3$ combustion, considering the advantages and limitations of green NH$_3$ synthesis. Studies have shown that pure NH$_3$ combustion presents challenges that must be addressed. Olabi et al. [20] explored the potential of NH$_3$ fuel in the energy sector and identified technical, economic, environmental, and regulatory hurdles that need to be overcome. Vries et al. [18] examined the current research status of various NH$_3$ applications as a green decarbonization fuel for heating, thermal power generation, and power equipment. Berwal et al. [19] reviewed the synthesis, chemical kinetics, and practical applications of NH$_3$ as a future combustion fuel, drawing insights from the combustion mechanism. Zamfirescu et al. [11] discussed and analyzed potential methods for using NH$_3$ as a sustainable fuel in FCs, evaluating efficiency and availability parameters based on the chemical reaction mechanism.

For power equipment that relies on thermal energy as the power source, the combustion chamber structure and combustion characteristics vary among different types of equipment, leading to distinct physical parameter requirements and pollutant emissions profiles for fuel. Similarly, for FCs that generate electricity through chemical reactions, each type of FC exhibits unique chemical reactions and optimal reaction temperatures, resulting in different pollutant emissions and corresponding mitigation strategies. Considering the diverse structures and operating principles of power equipment, this paper provides a comprehensive overview of NH$_3$ utilization as a decarbonization fuel and the associated pollutant emission reduction measures. It categorizes the output performance and pollutant emission characteristics of different power equipment, summarizes the challenges faced by NH$_3$ application, and presents an outlook on the future of NH$_3$ as a power source. The following sections delve into the NH$_3$ fuel application and NO$_x$ emission characteristics

of spark plug ignition (SI) engines, compression ignition (CI) engines, and gas turbines (GTs) from various aspects of operating conditions (e.g., mixed fuel, fuel-to-exhaust ratio, and equivalence ratio), structure and strategy (e.g., number of spark plugs, compression ratio (CR), fuel injection, and ignition mode), and auxiliary combustion techniques (e.g., preheating, humidification, exhaust gas recirculation, and secondary air supply). Meanwhile, the paper also reviews the output performance of different ammonia fuel cells under chemical combustion and flame combustion, especially the system efficiency and emission of indirect ammonia fuel cells based on supply from different heat sources (burning NH_3 combustion, anode tail gas combustion, and NH_3 decomposition gas). These findings will provide valuable insights for the development and application of NH_3 FCs.

2. Ammonia Used in Spark Ignition Engines

2.1. Mixing Fuels with Strong Activity

In SI engines, the fuel is compressed to the appropriate pressure and temperature for ignition through piston movement. High-energy spark plug injection ignites the fuel, causing it to expand and perform work, as illustrated in Figure 3. As a result, alternative fuels must have strong anti-knock properties and readily form a uniform mixture with air. NH_3 possesses excellent anti-knock properties, making it a promising carbon-free green energy source for SI engines. However, the development of NH_3 fuel in SI engines is hindered by its unfavorable physical properties. Several researchers, including Cornelius et al. [28], Starkman et al. [29,30], Cornelius et al. [22], Liu et al. [31], and Grannell et al. [32], have experimentally investigated NH_3 as a fuel for SI engines. Their findings indicate that pure NH_3 faces challenges such as inefficient flame propagation, difficult ignition, and unstable combustion, making it challenging to operate effectively in SI engines. Furthermore, NO_x and unburned NH_3 emissions are relatively high when using pure NH_3.
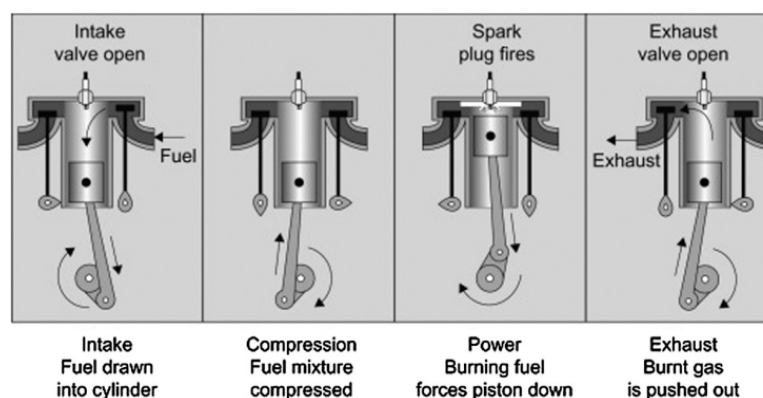

Figure 3. Typical 4-stroke SI internal combustion engine [11].

2.1.1. Combustion and Emission of NH_3/Gasoline SI Engines

Gaseous ammonia is pre-mixed with high-pressure ejected gasoline for 5 h, then mixed with a certain amount of air and injected into the cylinder through a direct ejector [33]. Supplementing NH_3 with reactive fuels is considered a crucial step in improving combustion stability and reducing the coefficient of variation (COV) of NH_3 combustion flame cycles [34]. For example, the laminar flame speed of NH_3 is limited to only 0.07 m/s [35], whereas that of gasoline is nearly 0.58 m/s. Therefore, incorporating gasoline into the mixture enhances flame propagation within the combustion chamber [25]. As mentioned earlier, SI engines rely on high-energy spark plug injection after compression to ignite the fuel. Consequently, the fuel should not self-ignite during the compression process, as this can lead to knocking and reduced SI output performance. NH_3's anti-knock properties enable NH_3/gasoline SI engines to operate at higher pressures, resulting in improved work efficiency [33]. While a high CR can significantly enhance the combustion characteristics of NH_3 fuel, a CR of 12:1 or higher is not recommended due to the intersection of the

minimum advance of the optimal torque detonation limit and rough limit crossover [36]. The schematic diagram of the ammonia and gasoline mixed-combustion test process as shown in Figure 4. On the other hand, mixing NH_3 with gasoline requires an increase in the ignition advance angle of the SI engine. A significant portion of the spark advance adjustment occurs when NH_3 contributes approximately 10% of the overall fuel energy input, but further increases in NH_3 content do not have any noticeable impact on flame speed [37].
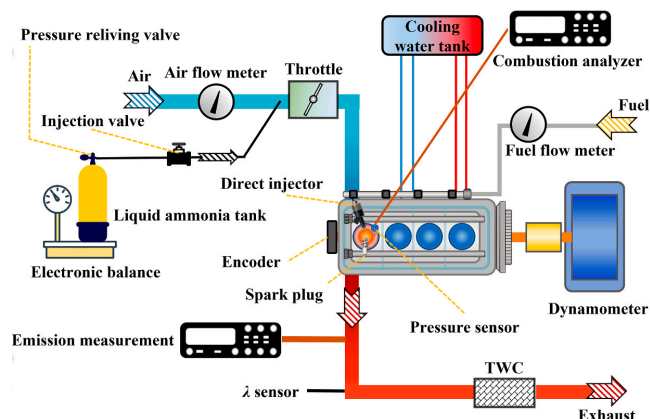
Figure 4. The schematic diagram of the ammonia and gasoline mixed-combustion test process [36].

Blending NH_3 leads to a deterioration in NO_x emissions due to fuel–NO_x formation. However, the sensitivity of NO_x emissions to the NH_3 blending ratio is generally moderate, and the trend of NO_x emissions with the ignition advance angle is opposite to that of pure gasoline, indicating that fuel–NO_x emission is strongly correlated with in-cylinder pressure [37]. Under high CR test conditions, Westlye et al. [38] found that NO_x was primarily produced during gap volume combustion and observed that NO emission levels were similar to those observed in gasoline measurements when the excess air coefficient (λ) is 1, mainly due to a lower flame temperature. The simulation involving the mechanism model revealed that the reaction between NH_2 and NO_2, as well as NH and NO, significantly influences the magnitude of this reaction, which is strongly influenced by the timing of ignition.

2.1.2. Combustion and Emission of NH_3/CH_4 SI Engines

CH_4, with its higher auto-ignition temperature and ability to form a more uniform mixture with air, is widely used in gasoline SI engines, requiring only minor modifications to the existing structure to meet operational requirements [27,28]. The physical properties of CH_4, such as density at room temperature, adiabatic combustion temperature, volumetric energy density, and octane number, closely resemble those of NH_3. Additionally, the laminar burning velocity of CH_4 combustion is over five times greater than that of NH_3 as a fuel. Therefore, combining NH_3 and CH_4 in combustion holds promising prospects for enhancing the combustion properties of NH_3. Compared with the pure NG engine, increasing X_{NH3} decreased the peak pressure (P_{max}) and HRR while increasing the best thermal efficiency (BTE) by 1%. NO_x emissions, originating from NH_3 at 873 K, initially increased with increasing X_{NH3} but then decreased [39]. The schematic diagram of the ammonia and natural gas mixed-combustion test process as shown in Figure 5.

Under high CR operating conditions, Zhang et al. [40] compared the performance and combustion characteristics of NH_3 fuel and CH_4 engines using a single-cylinder SI engine and verified the decrease in engine performance caused by physical properties such as flame propagation speed and the ignition difficulty of NH_3 fuel. Thermal imaging of combustion flame propagation indicated that the primary reason for the decrease in performance is the increase in the stagnant time of the NH_3 combustion flame during the initial flame development process. While the flame propagation of CH_4 is highly sensitive to temperature, NH_3 flame propagation is primarily influenced by turbulence [41].

Kurien et al. [42] investigated the effects of X_{NH3} and workload on the combustion stability of SI engines fueled by NH_3/CH_4 blends. At a low engine load of 8 Nm, increasing X_{NH3} from 0 to 60% reduced the laminar burning velocity and flame propagation speed of the fuel mixture, causing the COV of indicated mean effective pressure (IMEP) to increase from 1.36% to 14.9%. Conversely, at a higher engine load of 16 Nm, increasing X_{NH3} from 0 to 60% narrowed the COV of IMEP from 14.9% to 4.3% [42]. The addition of NH_3 reduces the combustion rate of the fuel mixture due to the lower combustion activity of NH_3, resulting in decreased peak pressure (P_{max}) and HRR [43]. High-speed camera images of flame propagation revealed that increasing X_{NH3} leads to a less wrinkled flame structure due to the addition of NH_3. This weakens the combustion reaction rate, lowers the flame speed, and ultimately reduces the intensity of turbulent combustion. The decrease in NO_x emissions is attributed to the lower combustion temperature caused by the addition of NH_3 [43].
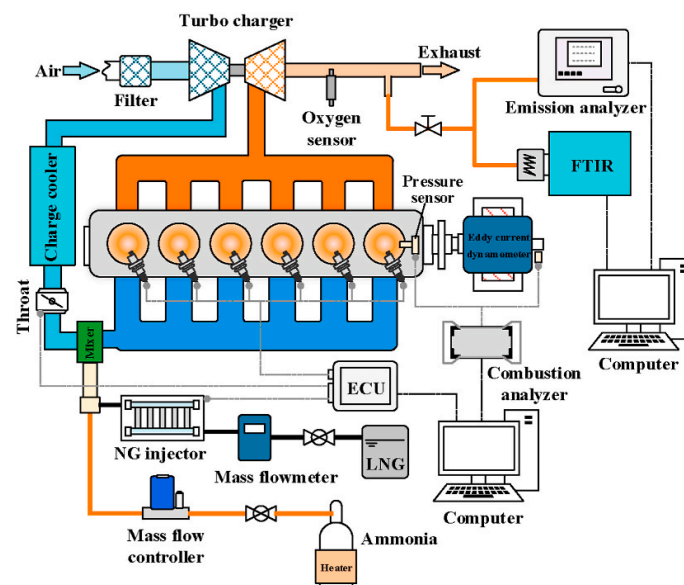
Figure 5. The schematic diagram of the ammonia and natural gas mixed-combustion test process [39].

Simulation studies have investigated the attenuation mechanism of CH_4 combustion induced by adding NH_3. Adding NH_3 fuel reduces the quantity of important radicals such as H and OH, leading to a decrease in the reaction rate of the fuel mixture. This causes a delay in the start of ignition (SOI) and prolongs the crank angles (CA) of 0~10° and 10~50° as X_{NH3} increases [43]. Increasing NH_3 also increases NH_3 slip, but it is beneficial that the slipped NH_3 effectively promotes NO reduction. Oh et al. [44] introduced fuel comprising a mixture of NH_3 and CH_4 into a modified six-cylinder SI and found that as X_{NH3} continued to increase, the amount of NH_3 slip increased and NO showed a trend of increasing first and then gradually reaching saturation. With the assistance of selective noncatalytic reduction (SNCR), NO emissions can be reduced to less than 10 ppm [44,45].

2.1.3. Combustion and Emission of NH_3/H_2 SI Engines

According to the data presented in Table 1, the flame propagation speed of H_2 is 3.5 m/s, approximately 50 times faster than NH_3's flame propagation speed. Despite NH_3 possessing good anti-knock properties, the octane number of H_2 is comparable to that of gasoline. Consequently, X_{H2} should not be excessively high. In the pursuit of determining the optimal X_{H2} threshold suitable for gasoline direct injection (GDI) engines, researchers [46] injected NH_3 and H_2 into the cooperative fuel research (CFR) engine manifold and investigated the impact of X_{NH3} on engine performance. Compared to traditional gasoline SI engines, efficiency and power witnessed a significant increase due to the potential for a higher CR. The findings also indicated that a fuel with $X_{H2} = 10\%$ exhibited the highest efficiency and power performance. When X_{H2} is lower than 60%, the deflagration tendency remains consistent at the boundary, but it changes significantly as X_{H2} increases continuously [46]. The optimal X_{H2} threshold of the NH_3/H_2 mixture is influenced by load and equivalence ratio. In the initial stages of combustion, H_2 demonstrated a particularly noticeable accelerating effect, serving as an ignition promoter. Blending H_2 with $X_{H2} = 20\%$ improved cyclic stability, prevented misfires, and resulted in optimal power output and indicated efficiencies comparable to stoichiometry. Increasing workload enhanced output performance and expanded operational limits concerning mixture composition [47].

Under high CRs of up to 13, the impact of adding H_2 on the combustion characteristics of NH_3 in a single-cylinder SI engine was analyzed. Additional H_2 was found to worsen indicated thermal efficiency, as the high-temperature combustion of H_2 resulted in significant heat transfer loss [48]. The visualization of combustion further revealed a critical threshold for the energy ratio between H_2 and NH_3. High-speed flame images depicting different H_2/NH_3 mixing ratios are shown in Figure 6. The addition of H_2 to the air–NH_3 mixture enhanced combustion speed, with optimal ratios being more dependent on engine load rather than speed. The NH_3/H_2 mixture was introduced into the intake manifold of a two-cylinder, four-stroke, low-speed marine engine. Experimental results [49] revealed that a minimum energy ratio of approximately $X_{H2} = 7\%$ was necessary for the engine to operate reliably at full load, while a ratio of 11% was required at half load. A proposed method involving the ignition of NH_3 with an H_2 jet flame successfully achieved full-load power output for the SI engine [49].
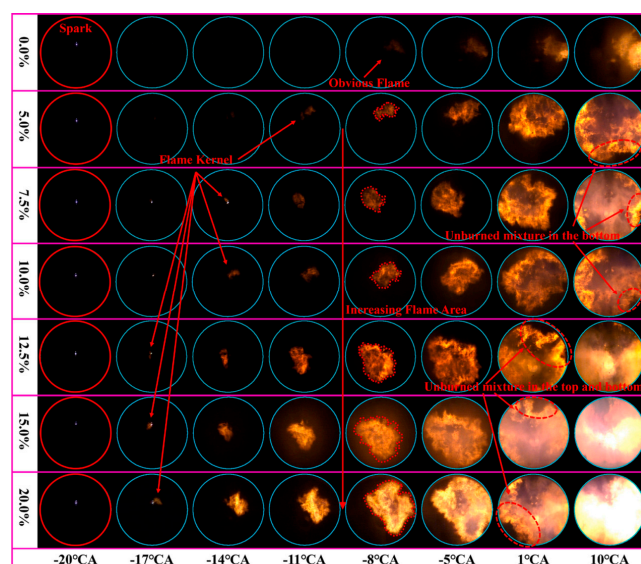

Figure 6. High-speed flame images of different H_2/NH_3 mixing ratios [48].

Similarly, in the quest for the optimal X_{NH3} threshold in NH_3/H_2 mixed fuel, when X_{NH3} exceeded 80%, it could induce flame instability and even misfire. Under lean combustion conditions, the engine's combustion performance is less sensitive to NH_3 fractions [50]. The detailed combustion and emission characteristics of NH_3-fueled SI mixed with other fuels under different operating conditions are outlined in Table 2.

Table 2. Combustion and emissions of NH_3-fueled SI with mixed fuel.

| Test Fuel	Baseline	Power Equipment	Operating Conditions	Performances	Emissions	Ref.
Gasoline/ NH_3	Gasoline	• CFR engine • 1-cylinder	• CR (7, 8, 9, 10) • 1600 rpm • IMEP (550 kPa)	Combustion duration ↓ 10 °CA, 40% gasoline power; best CR = 10.	-	[32]
NH_3/H_2	Gasoline	• CFR engine	• CR (7~15) • 1000 rpm • λ (1~1.4) • Full throttle • X_{NH3} = 80%	-	NO ↓ 1500 ppm as SOI = 30 °CA BTDC. NO_2 ↑ 100 ppm, N_2O ↓ 50 ppm as SOI ↑ 40 °CA.	[38]
NG/NH_3	NG	• 6-cylinders • 4-stroke • turbocharged • premixed • 4-valve	• CR = 11.5 • X_{NH3} (0~60%) • λ (1.1~1.5)	X_{NH3} ↑, CP ↓, combustion duration ↑; λ = 1.3 and X_{NH3} = 30%, optimum BTE; λ = 1.1, X_{NH3} = 50%, max HRR.	X_{NH3} ↑, NH_3 and N_2O ↑; X_{NH3} = 30%, λ = 1.2, NO_x (6000 ppm).	[39]
NG/NH_3	NG	• NG engines • 6-cylinder • premixed • turbocharged	• CR = 10.5 • 1~100 rpm • Max load • X_{NH3} (0~50%) • λ (0.9~1.6)	λ ↑, BTE ↑; X_{NH3} ↓ BTE ↑; Max BTE = 41.7%, λ = 1.5.	X_{NH3} ↑, NO_x →; NH_3 slip ↓, NO ↑.	[44]
H_2/NH_3	H_2	• 4-stroke • 4-cylinder	• 1500 rpm • CR = 10.7 • X_{NH3} (10~80%) • λ (1, 1.4)	X_{NH3} ↑, BMEP ↑, BTE ↑; max BTE X_{NH3} (60~70%); limit X_{NH3} = 80%.	X_{NH3} = 20%, max NO_x = 8000 ppm.	[50]
H_2/NH_3	Gasoline	• 4-stroke • 2-cylinder	• CR = 10.7 • 2500~5000 rpm • λ = 1 • Full load • H_2/NH_3 = 6~8%	BTE ↓ 2.5% regardless of engine speed; BP ↓ 3 kW (3500 rpm); NH_3 has certain demerits as a fuel load.	Full load NO_x ↓ 1000 ppm.	[49]
H_2/NH_3	NH_3	• 1-cylinder • 4-stroke • 4-valve	• CR = 10.5 • 1500 rpm • H_2 share (0~60%) • λ (0.6~1.2) • Engine loads (CP = 0.1 MPa, 0.12 MPa); • Direct injection	λ ↑, PMEP ↑, combustion duration ↓, best X_{H2} = 20%; engine load ↑, operating boundaries ↑.	X_{H2} ↑, NO_x ↑, NH_3 slip ↓.	[51]
$H_2/NH_3/CH_4$ (any two)	H_2/CH_4	• 4-stroke • single-cylinder • premixed	• CR = 10.5 • 1500 rpm • X_{H2} (0~15%), XCH_4 (5~15%)	$NH_3/15\%H_2$, max peak HRR = 31.2; 100% CH_4, min peak HRR = 10.5.	-	[52]
H_2/NH_3	H_2/NH_3	• 1-cylinder • 4-stroke (modified from a CI engine)	• CR (8~15) • X_{H2} (5~21%) • 1400/1800 rpm	X_{H2} from 5% to 21%, BP ↑ 16.89%, BTE ↑ 33%, volumetric efficiency ↓ 13.64%.	X_{H2} ↑, peak temperature ↑, NO_x ↑.	[53]

↓, ↑ and → are down, up, unchanged respectively.

2.2. Structure Adjustment and Auxiliary Combustion Measures

2.2.1. Structure Adjustment and Strategy

The enhancement of combustion stability, flame propagation speed, and reduction of NO_x emissions can be further achieved with the implementation of operation and control strategies [24]. The injection strategy of pilot fuel proves effective in reducing the minimum ignition energy of NH_3 mixed fuel. This aids in establishing conditions for the formation of H and OH radicals, thereby shortening the initial stagnant time of NH_3 combustion [54]. The vaporization of liquid NH_3 demands a substantial amount of energy, leading to a significant decrease in the temperature of the air introduced into the cylinder. This, in turn, hinders the subsequent propagation of the turbulent flame, resulting in a decline in combustion efficiency or even potential misfire. Preheating proves beneficial by increasing the saturated vapor pressure, raising the initial temperature, and accelerating the reaction rate of fuel combustion [55]. Preheating also impacts NO_x emissions, as illustrated in Figure 7.
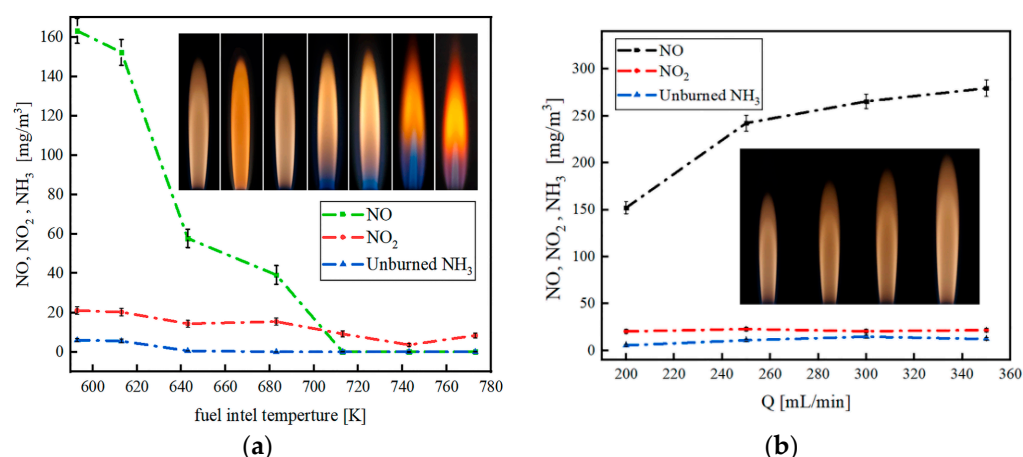
Figure 7. The emissions with different preheating temperatures (**a**) and NH_3 flow rates (**b**) [55].

Implementing a direct injection system, which mixes fuels and injects the mixture directly into the cylinder, eliminates the volume of the intake manifold and improves volumetric efficiency. Ryu et al. introduced a direct injection system in a CFR engine operating at 1800 rpm [56]. The engine output ranged from 1.25 to 2.75 kW, slightly lower than when using gasoline alone. Consequently, the higher levels of NH_3 observed in the exhaust did not indicate a decline in combustion efficiency but rather reflected a greater supply of NH_3. The key factor in improving combustion performance lies in the regular injection of the mixed fuel into the cylinder.

Pandey [57] compared the impact of ignition time on the combustion performance of an engine using a NH_3/H_2 mixture and pure H_2 as fuel. This study utilized a 0.661 L, four-stroke, one-cylinder SI engine. The findings revealed that increasing the delayed ignition angle decreased the in-cylinder pressure of the NH_3/H_2 mixture and delayed P_{max}. The sensitivity of in-cylinder pressure to the ignition angle was weak when H_2 was burned. The peak of the HRR for the NH_3/H_2 mixed fuel occurred behind the top dead center (TDC), while the combustion of H_2 mainly occurred in front of the TDC. The delay angle tended to result in a delayed peak value of HRR, typically elevating the in-cylinder pressure of pure H_2. Whether it was an NH_3/H_2 mixture or pure H_2, thermal efficiency was closely related to NO_x emissions [57], as verified by [46].

Xin et al. [58] investigated the effect of variable valve timing (VVT) on a water-cooled, four-stroke, four-cylinder SI engine provided by the direct injection system under the Miller cycle. Advancing the intake valve timing and maintaining a larger valve overlap angle led to a decrease in combustion stability, an elongated flame development period (0–10 °CA), an increase in COV, an exceedance of MAX_{COVP} beyond 25%, and a rapid drop in BTE from 32.8% to 30%. However, retarding the intake valve timing by 25 °C increased IMEP and

BMEP by 8% and 16%, respectively. Based on this research, advancing the intake valve timing is unsuitable for the Miller cycle H_2-enriched NH_3 engine [50,58,59].

In their comparison of control strategies on NH_3-fueled SI engines, Xin et al. [50] evaluated three load control strategies: throttle, NH_3/H_2 mixing ratio, and equivalence ratio. Experimental research revealed that controlling the throttle broadened the engine's output power threshold, enhanced BMEP, and maintained thermal efficiency above 33%. The NH_3/H_2 mixing ratio strategy, due to the fast propagation speed of the H_2 flame, proves suitable for cold start conditions. The strategy of controlling the equivalence ratio can achieve higher thermal efficiency [59]. Hong et al. [60] investigated the effects of various load control strategies on the performance of NH_3-fueled SI engines. Qualitative control of VVT combined with quantitative control enabled the engine to meet a wide range of BMEP regulations while maintaining BTE above 37% in most cases. As the air/fuel ratio increased from 1.0 to 2.0, BMEP and P_{max} gradually decreased due to reduced fuel flow in the cycle. After increasing the air/fuel ratio, BTE initially increased and then decreased rapidly, reaching its maximum value of 39% when the air/fuel ratio was 1.4 [60].

Improving the CR is also a crucial measure for enhancing engine performance [37,61,62]. According to [63], the study found that increasing the CR from 9.41 to 11.51 increased P_{max} by 59%. Additionally, under supercharged conditions, introducing 10% H_2 into the mixture improved indicated efficiency by 37%. As the CR increased from 8 to 15, flame development accelerated, shortening the combustion period. Increasing X_{H2} from 5% to 21% improved brake power and increased BTE by 16.89% and 33%, respectively, at 1400 and 1800 rpm, but decreased volumetric efficiency by 13.64%. However, with increasing X_{H2} and CR, the exhaust temperature decreased, and the influence of X_{H2} on the exhaust temperature diminished [64]. Despite the relatively small amount of thermal NO_x generated by fuel combustion, where fuel NO_x was the primary component, an increase in X_{H2} led to a continuous rise in NO_x due to the heightened peak temperature resulting from the addition of H_2 [53].

The addition of mixed H_2-rich reforming gas serves to increase the concentration of H and OH radicals, consequently elevating in-cylinder pressure and shortening the combustion duration. The introduction of 10% H_2-rich reforming gas improves combustion efficiency by 96.3% and thermal efficiency by 43.6%. However, when the mixing ratio exceeds 12.5%, the negative impact becomes more pronounced [64]. Increasing the CR yields higher in-cylinder pressure and temperature, enhancing NH_3 combustion and engine output performance while creating conditions conducive to NO_x generation. Thus, striking a balance between engine output performance and NO_x emissions is crucial. Auxiliary combustion technologies, such as exhaust gas recirculation (EGR), prove effective in improving engine output performance while maintaining NO_x emissions within a controllable threshold [65–67].

2.2.2. Auxiliary Combustion Measures

Developing the application of NH_3 fuel with minimal mechanical modifications to a given engine is a key focus [56,68], as are auxiliary combustion measures. Upon examining the impact of EGR on combustion performance by varying EGR rates from 0 to 25, it was found that pure H_2 exacerbated combustion instability compared to the NH_3/H_2 mixture at higher EGR rates [57]. Implementing an initial EGR rate enhances the mean gas temperature by heating the intake with recirculated gases, thereby improving fuel combustion, boosting flame velocity, and enhancing the conversion of NH_3 to N_2. In summary, with the assistance of EGR (above 15%), the combustion stability advantage of NH_3/H_2 mixed fuel is significant [57]. This was attributed to the fast combustion rate of pure H_2 and its shorter stagnant time compared to the NH_3/H_2 mixture, which explains the significant reduction in NO_x emissions in the NH_3/H_2 mixture under highly delayed ignition conditions.

Increasing the number of spark plugs effectively reduces NO_x emissions while enhancing flame propagation speed. Uddeen et al. [69] modified the existing engine ignition system to equip it with four spark plugs, which showed that multi-spark-plug ignition pro-

motes flame propagation, shortens the initial flame retention time, and improves the pure NH_3 combustion rate. However, it increases in-cylinder pressure and temperature, creating an unfavorable environment for NO_x formation. To enhance combustion performance, Liu et al. [70] employed pre-chamber turbulent jet ignition (TJI) technology on a 0.5 L, one-cylinder, four-stroke SI engine with a CR of 14, as shown in Figure 8. TJI generates turbulent jet flames, enabling multi-point ignition and stable combustion for low-reactivity fuel mixtures in the combustion chamber [70]. Adopting the TJI mode shortens combustion time and delays ignition time owing to an increase in ignition energy, which is beneficial to improving the combustion stability of the NH_3 SI and increasing the combustion rate. Regardless of the ignition method, the NO_x and NH_3 emissions of NH_3 SI engines are higher [70].
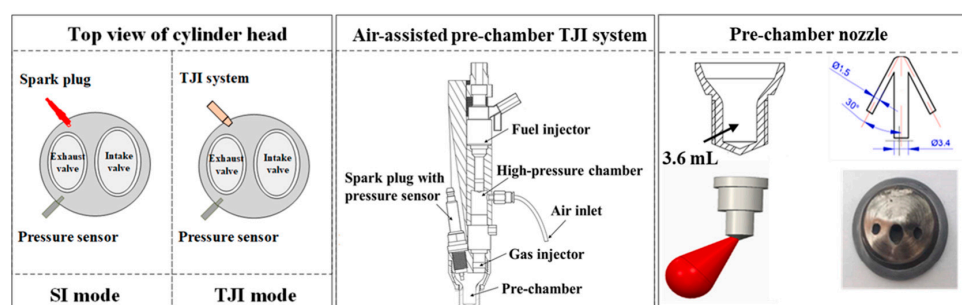
Figure 8. The basic configuration of the TJI system [70].

The instability of NH_3 combustion poses challenges for cold-starting NH_3 SI engines. Koike et al. [71] pioneered the use of H_2-rich reforming gas (resulting from the online thermal decomposition of NH_3) for cold-starting an SI engine. Achieving a fast cold start was possible when the NH_3/H_2 mixing ratio was 1:2, and stable operation was maintained under no-load conditions. To address the emissions of unburned NH_3 during the cold start and transition to stable operation, it is crucial to implement post-treatment measures for emissions. Test results indicated that with the assistance of a three-way catalyst, NH_3 emissions were close to zero [71]. The detailed combustion and emission characteristics of NH_3 SI engines, assisted by changes in structure and strategy, are presented in Table 3.

In summary, the pathways to enhance combustion and reduce emissions in NH_3 SI engines are illustrated in Figure 9. The addition of other fuels results in a significant increase in flame propagation speed, a reduction in the flame stagnation time during the initial stage of combustion, and a notable improvement in BTE. However, this comes at the cost of a substantial increase in fuel–NO_x emissions. Altering the structure of an SI engine or adjusting fuel injection or ignition timing can effectively raise pressure and temperature in the cylinder, leading to a significant upward trend in engine BTE. Nevertheless, NO_x emissions and NH_3 slip are not satisfactorily addressed. The incorporation of auxiliary combustion technology proves effective in enhancing NH_3 combustion efficiency and consequently reducing NO_x emissions.

Table 3. Combustion and emission of NH_3-fueled SI engines assisted by changing the structure and strategy.

Test Fuel	Baseline	Power Equipment	Operating Conditions	Performance	Emissions	Ref.
NH_3/CH_4	CH_4	• 1-cylinder • 4-stroke • 2-spark plug	• CR = 10 • 1500 rpm • X_{NH3} (0~60%) • load (8 Nm to 16 Nm) • λ = 1	X_{NH3} ↑, engine performance ↓; X_{NH3} ↑ (0 to 60%), COV of IMEP ↑ (1.36% to 14.9%); operating load ↑, COV_{IMEP} ↓ (14.9~4.3%), combustion stability ↑.	NH_3 ↓ by the SCR.	[42]
NG/NH_3	NG/NH_3	• 6-cylinder • turbocharged • premixed	• 840 rpm • λ (1.2~1.5) • split ratios (0~50%)	λ is limited to 1.5; λ and split ratio of NH_3 ↑, burn duration ↓.	fuel-NO_x dominated the total emission; λ and split ratio of NH_3 ↑, NO_x ↑.	[45]
H_2/NH_3	Gasoline	• CFR • GDI	• 1200 rpm • λ > 1 • NH_3/H_2 share: 90/10	ITE ↑ by 0.5% as CR ↑ by 2.6.	NO_x emission was 5500 ppm (CR = 8.9, λ = 1.3~1.4, H_2/NH_3 volume ratio = 70/30).	[46]
H_2/NH_3	H_2	• 1-cylinder • 4-stroke • premixed	• CR = 15 • Ignition (−24 °CA to ~12 °CA) • EGR rates (0~25%)	EGR rate helps to improve HRR, CP; best EGR rate = 7.5.	EGR ↑, NO_x has a parabolic descent.	[57]
H_2/NH_3	H_2/NH_3	• 4-cylinder • 4-stroke	• CR = 10.7 • 1500 rpm • λ = 1 • X_{NH3} = 70% • 60% throttle opening	Intake valve timing ↑, combustion stability ↓, °CA 0–10 ↑, MAX_{COVP} ↑ 25%, BTE ↓ (32.8~30%); Intake valve timing ↓ 25 °CA, IMEP ↑ 8% and BMEP ↑ 16%.	-	[58]
H_2/NH_3	H_2/NH_3	• 4-cylinder • 4-stroke • 4-load control strategies	• CR = 10.7 • 1500 rpm • NH_3/H_2 ratio (10–70%) • λ = (1~1.7) • VVT (−20 to −25) °CA	Air/fuel ratio: BTE ↑ to 40%; Throttle: the widest power range.	-	[59]

Table 3. *Cont.*

Test Fuel	Baseline	Power Equipment	Operating Conditions	Performance	Emissions	Ref.
H_2/NH_3	H_2	• 4-cylinder • GDI	• CR = 10.7 • 1500 rpm • NH_3 share (0–70%) • λ (1~2)	BTE ↑ 37%; MAX_{COVP} is raised to nearly 9% when X_{NH3} is 70%; Peak BTE close to 39%, MAX_{COVP} below 4% when λ is 1.4.	NO_x above 8000 ppm.	[60]
NH_3	NH_3	• 1-cylinder • 4-spark plug • GDI	• CR = 10.5 • Spark timing (−35, −30, −25, −20)	CP ↑; Combustion duration ↓; Combustion stability ↑; Combustion rate ↑; Engine power ↑.	T ↑, NO_x ↑.	[69]
NH_3	NH_3	• 1-cylinder • 4-stroke • TJI	• CR = 14 • Intake temperature (300 K, 343 K)	Combustion stability ↑, in-cylinder pressure ↓, and the peak of HRR ↑.	Lower NO by TJI.	[70]
Gasoline/ H_2/NH_3	Gasoline/ NH_3	• 1-cylinder • CFR engine • 4-stroke • GDI	• CR = 10 • 1800 rpm • $m_{gasoline}$ = 27.5 g/min • m_{NH3} = 3.75~13.85 g/min	BP ↑~0.2 kW Brake Specific Energy Consumption ↓ 5 MJ/kWh.	NO_x ↓ 25 g/kWh (m_{NH3} = 7.2 g/min) NH_3 slip ↓ 83%. (m_{NH3} = 7.2 g/min).	[72]
H_2/NH_3	NH_3	• 2-cylinder • 4-stroke • 2-valve	• CR = 10.7 • 2500~3500 rpm • Full throttle • λ = 1 • m_{H2} = 2 g/min • m_{NH3} = 88.5–93.6 Nm^3/h	BTE ↓ 3% (2500 rpm); BTE ↑ 1.5% (3500 rpm).	NO_x ↓ 1000 ppm. High load NO_x > half load NO_x by 200 ppm.	[73]

↓ and ↑ are down and up, respectively.
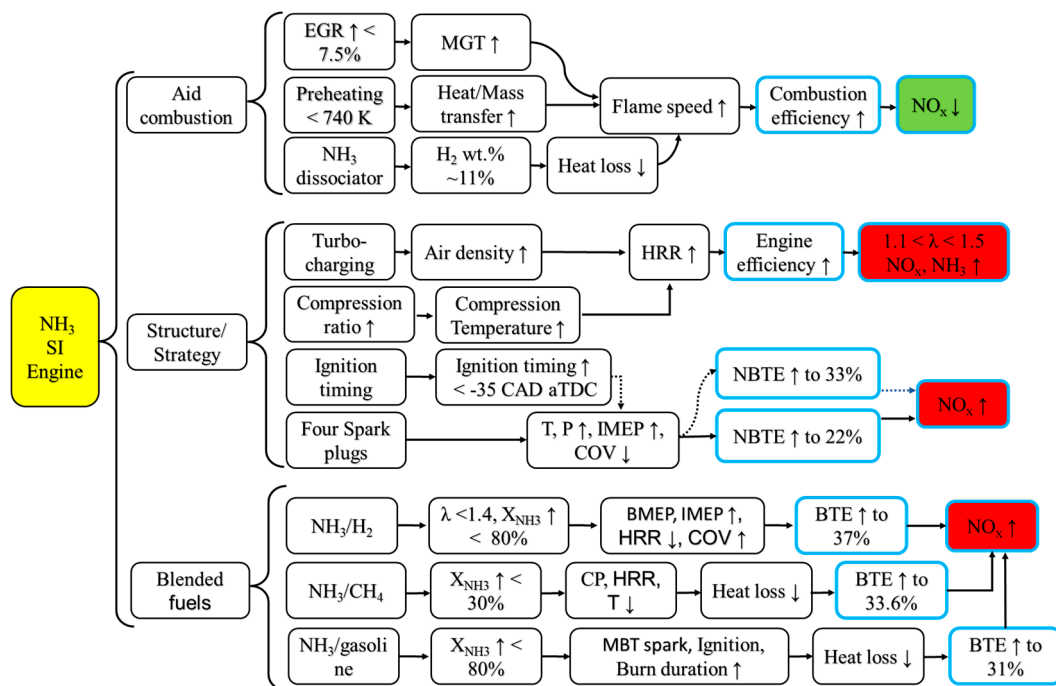
Figure 9. Pathways to promote combustion and emission reduction in NH$_3$ SI engines. ↓ and ↑ are down and up, respectively.

2.3. Exhaust Gas Aftertreatment to Minimize NO$_x$ Emissions from SI Engines

For traditional fuel SI engines, NO$_x$ emissions can meet relevant emission standards through some structural improvements and some operational strategy optimizations. For NH$_3$ fuel engines, fuel–NO$_x$ is a major component of NO$_x$ emissions. It is necessary to adopt after-treatment of emissions similar to SCR systems to make NO$_x$ emissions meet emission standards [74]. Ammonia is a common reducing agent for NO$_x$, so the presence of unburned ammonia fuel in the exhaust is beneficial to reducing NO$_x$ emissions. Studies show that rich conditions can lead to elevated ammonia levels, while nitrous oxide generation remains low in all circumstances [75]. In addition, in order to reduce the problem of low fuel utilization caused by rich combustion, Vitaly et al. used a lean SI engine to install an ammonia device that can store upstream generated ammonia on the original supporting aftertreatment system platform, thereby achieving the effect of reducing NO$_x$ emissions [76].

When pure NH$_3$ or NH$_3$ mixed with other active fuels is burned, NO$_x$ emissions increase significantly, but the advantage of ammonia as a nitrogen oxide reducing agent increases. Oh et al. [44] used the aftertreatment system of the original SI engine, including a selective catalytic reduction system and an ammonia oxidation catalyst, to study the characteristics of nitrogen oxides and residual ammonia before and after the exhaust flow through SCR under different air/fuel ratios and fuel mixing ratios, and found that as the ammonia energy fraction increased, the temperature during combustion decreased significantly. Although the fuel–NO$_x$ emissions increased, the NO$_x$ emissions after passing through the SCR system tended to be saturated. At the same time, it was found that the remaining ammonia can reduce the NO in the exhaust gas before passing through the SCR at a suitable temperature. When passing through the SCR system, the remaining ammonia will reduce the remaining NO again, and the final NO emission can be controlled within 10 ppm. Other NO$_x$ emissions are less than hundreds of ppm. After the remaining ammonia acts as a NO$_x$-reducing agent repeatedly, the residual ammonia is within 10 ppm.

3. Ammonia Used in Compression Ignition Engines

The air injected into the cylinder undergoes compression to reach a specific temperature and pressure due to piston movement. Subsequently, fuels are introduced into the cylinder through atomization, ignition, and expansion [77]. For CI engines, the fuel must possess good auto-ignition performance and a short ignition delay period [78]. The challenging ignition characteristics of NH_3 make its normal operation in CI engines more difficult than in SI engines.

NH_3 has the most significant impact on improving the ignition delay period of diesel, while it has the smallest effect on improving P_{max} and efficiency. Several potential strategies for using NH_3 as a CI fuel include (a) blended fuel combustion [79], (b) high CR [80], and (c) injection strategies [81,82]. Overcoming the combustion challenges of NH_3 fuel often requires a combination of these measures. An effective strategy to enhance the combustion performance of NH_3 is to blend it with a more reactive fuel. Similar to SI engines, if the auto-ignition temperature of the fuel is higher than the cylinder temperature at the end of compression, it can be mixed with NH_3 fuel and injected into the combustion chamber of the CI engine to mitigate the defects in the physical characteristics of NH_3 fuel. The engine's performance during combustion heavily depends on the cetane number (CN) of the mixed fuel, where a higher CN results in optimal performance with shorter ignition delays and optimum combustion efficiencies.

3.1. Mixing Fuels with Strong Activity

3.1.1. Combustion and Emission of NH_3/Diesel CI Engines

Regardless of whether NH_3 fuel is supplied to the engine in a liquid or gaseous state, it can meet typical engine load and thermal efficiency requirements through a blended fuel premix mode ignited by the pilot fuel [83]. The release of heat is faster in the case of liquid NH_3, leading to higher cylinder pressure. Compared to liquid NH_3, the HRR decreases by 50% and 25% and the pressure reduces by 6.5% and 11.5% under the energy supply of gaseous NH_3 at 100% and 80%, respectively. Unfortunately, NO_x emissions far exceed Tier III limits [83]. For achieving the same output power as diesel in CI engines, the intake manifold of a four-cylinder CI engine is slightly modified to be suitable for the direct NH_3/diesel injection strategy. As the X_{NH3} increased, the CA corresponding to the P_{max} in the cylinder also increased while the peak value gradually decreased (from 9.5 to 7.5 MPa). Additionally, the HRR showed a significant increase (from 0.04 to 0.1), and the emission of NO under blended-fuel operation ($X_{NH3} < 40\%$) decreased significantly, resulting in lower thermal NO emissions but higher fuel–NO emissions ($X_{NH3} > 60\%$) [84]. The performance of a CI engine fueled by a NH_3–diesel blend as shown in Figure 10. By adopting a split diesel injection strategy (SODI), combustion thermal efficiency has been increased to 39.72% but also a resulting 83.5% decrease in unburned NH_3 emissions, surpassing that of pure diesel [78]. Leveraging the advantages of the split fuel injection strategy, optimizations such as SODI-pre and SODI-main can be implemented [85]. By reasonably controlling the injection time of diesel and NH_3, the NH_3 combustion speed could be accelerated, maintaining liquid NH_3 in a stable state throughout the entire combustion stage [86].

Achieving a high injection pressure is crucial to ensuring effective atomization of the fuel mixture [87]. Zhou et al. [88] developed a combustion model for a CI engine under the high-pressure direct fuel injection mode (HPDF). Compared to the commercial low-pressure, blended-fueled direct fuel injection mode (LPDF), this mode can reduce NO_x emissions by approximately 47% while maintaining the same thermal efficiency. Utilizing the same spray device, Zhu et al. [89] determined that the NH_3 addition threshold is unsuitable for exceeding 40%, considering the impact of NH_3 addition on ignition delay, premixing efficiency, and NO_x emissions [88]. CI ignited by the pilot fuels under two modes as shown in Figure 11.
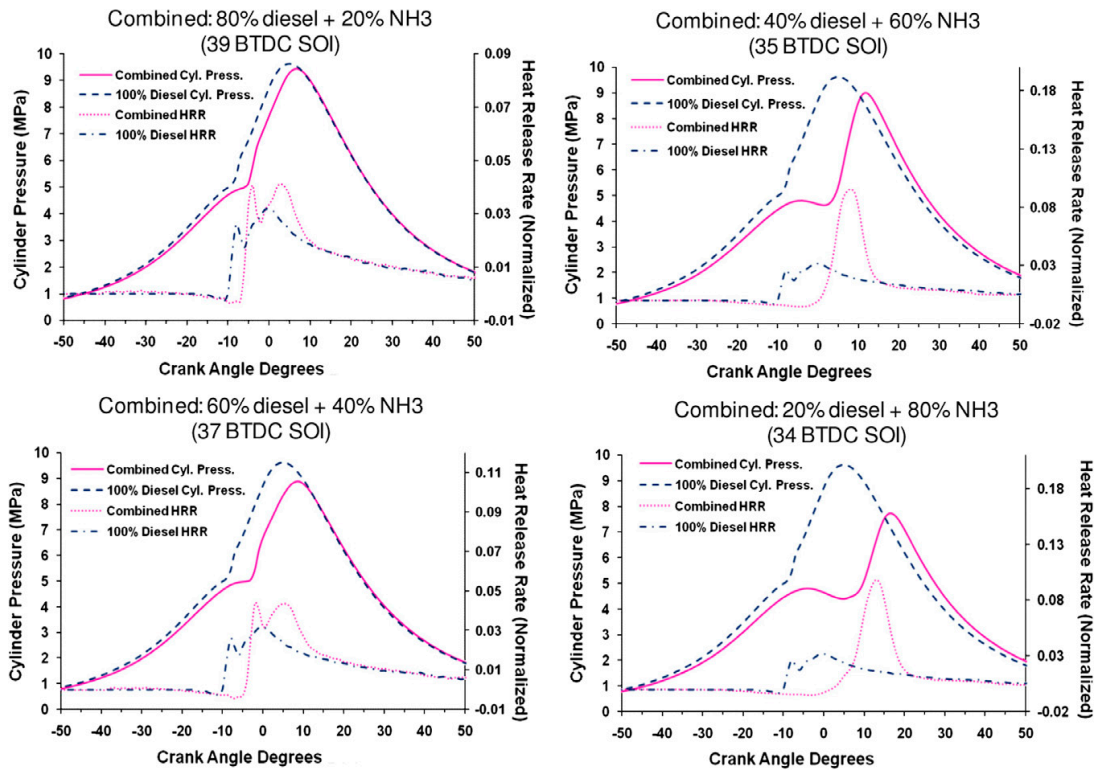
Figure 10. The performance of a CI engine fueled by a NH_3–diesel blend [84].
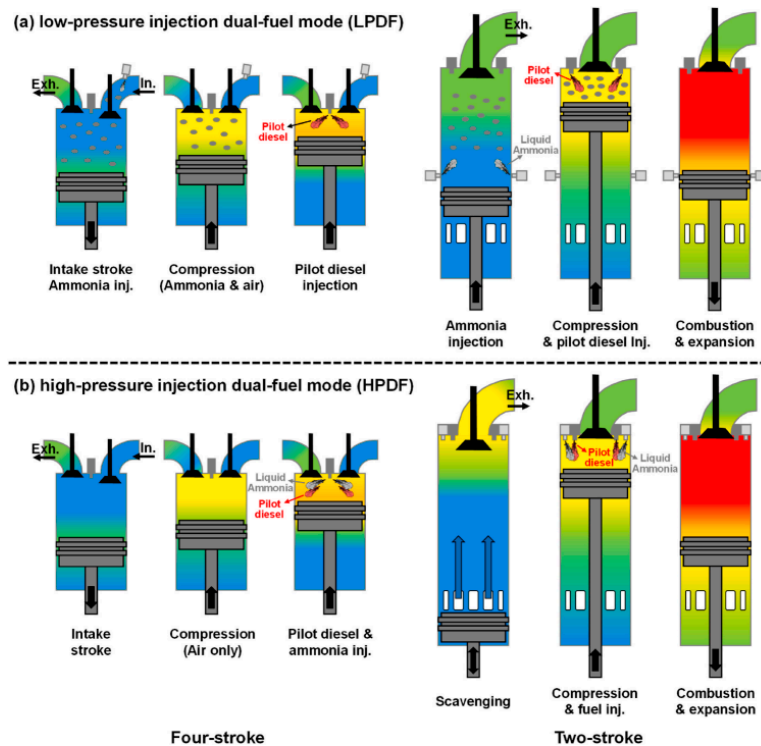

Figure 11. CI ignited by the pilot fuels under two modes [88].

Numerical simulation results have successfully validated the feasibility of the new high-temperature cylinder gas recirculation (HTCGR) technology [88]. The new HTCGR technology as shown in Figure 12. Consequently, it is crucial to investigate the impact of mixing combustion-generated water with NH_3 on engine combustion and emissions. Frost et al. [90] conducted combined numerical analysis and experimental research to explore the effects of different concentrations of NH_4OH (ammonium hydroxide) on CI combustion under various workloads. At an IMEP of 4 bar, although the ignition delay time is longer than that of pure diesel, NH_3 can be ignited and contribute 25% of the engine load. Increasing NH_4OH concentration increases NO_x emissions, as the elevated cylinder temperature during this stage is closely related to NO_x emissions. After continuously increasing NH_4OH concentration and contributing 20% to the engine load, NO_x levels decrease. Excessive NH_3 concentration increases combustion instability and lowers the in-cylinder temperature [91]. These findings align with results in the literature [92], where the addition of a NH_3 solution reduces combustion pressure and HRR, increases engine diameter and ignition delay, reduces engine performance, and significantly decreases NO_x emissions.
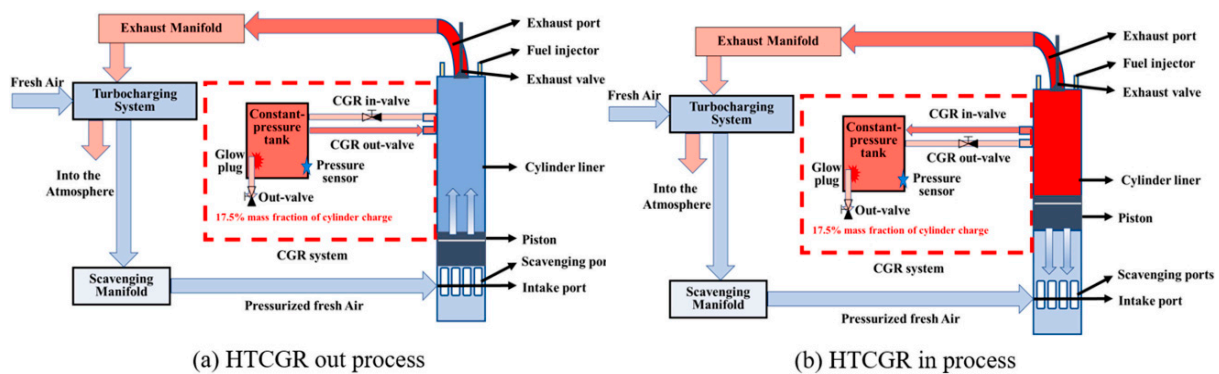
Figure 12. The new HTCGR technology [81,88].

In addition to the NH_3 energy ratio, factors such as engine speed and load also influence engine combustion and emissions. Shahin et al. [93] studied the impact of NH_3 energy ratio, speed, and load on combustion and emissions. In the medium load range, total fuel consumption, as measured by specific fuel consumption, decreased with increasing load. Additionally, the presence of air fuel (NH_3 injection in the air) resulted in an increase in total fuel consumption under slightly higher load conditions, with a similar trend observed for NO_x emissions. Optimal outcomes regarding engine performance and exhaust emissions were observed for NH_3 fumigation at 2600 rpm. Under 8 Nm and 2600 rpm, the maximum effective efficiency increased by 15.05% with an air/fuel ratio of 8.5% [93]. A mixture of 25% NH_3 and 75% water solution was used and injected into the intake through a carburetor with an adjustable main nozzle. It was proven that NH_3 can reduce NO_x by more than 70% in the parameters analyzed, while the effect on brake-specific consumption is negligible. Compared to pure diesel CI, the mixture (with 10% H_2 content) increased peak pressure by 5.3% and maximum temperature by 5.7% [94]. Combustion and emission of a NH_3 CI engine with mixed fuel, as shown in Table 4.

Table 4. Combustion and emission of a NH_3 CI engine with mixed fuel.

| Test Fuel	Baseline	Power Equipment	Operating Conditions	Performance	Emissions	Ref.
NH_3/diesel	diesel	• 4-cylinder • Turbocharge • direct injection	• X_{NH3} (20~80%) • constant power output operation	Combustion efficiency range of 91~97%; power output is same; HRR ↑ (0.04~0.1).	NH_3/diesel (60%/40%), NH_3 = 3200 ppm; NO ↓.	[84]
aqueous NH_3/diesel	diesel	• 4-stroke • 1-cylinder • direct injection	• CR = 15.5 • 100% load • X_{NH3OH} (40%, 50%, and 60%)	pressure ↓ (16.4%, 20.2%, 22.7%), peak value of HHR ↓ (29.8%, 45.6%, 64.9%), brake power ↓ (36.3%, 45.3%, 54.5%) at X_{NH3} ↓ (40%, 50%, 60%).	NO_x ↓ 25%, 52.3%, and 61.8%, respectively.	[91]
aqueous NH_3/diesel	diesel	• 1-cylinder • 4-stroke • direct injection	• CR = 20 • 2200, 2600 and 3000 rpm • X_{NH3} (2, 4, 6, 8, 10%) • Engine loads of (2, 4, 6, and 8) Nm	Effective efficiency ↑ 15.05% (8.5% AF ratio, 8 Nm, 2600 rpm).	NO_x emissions are about 1.5 times that of 4 Nm and 2.5 times that of 2 Nm.	[93]
NH_3/DME	DME	• 1-cylinder • 4-stroke • Direct injection	• CR = 20 • X_{DME} (100%, 80%, 60%, 40%) • CAD (10~15, 10~20, 15~30)	P (X_{NH3} = 40%) is higher; the peaks of HRR increase with X_{NH3}.	NO_x of mixture (20% NH_3, 80% DME) is higher.	[95]
NH_3/DME	DME	• 1-cylinder • 4-stroke • High-pressure common rail • direct injection	• CR = 20 • X_{DME} (100%, 80%, 60%, 40%)	X_{NH3} ↑, injection timing ↑; engine performance decreases as X_{NH3} ↑.	NH_3 concentration ↑, NO_x emissions ↑, NH_3 emissions ↑	[96]
NH_3/H_2(HCCI)	H_2	• 1-cylinder • 4-stroke	• CR = 21.9 • X_{NH3} (0 to 94%) • ER (0.1 to 0.6) • T (50 to 240 °C) • EGR	X_{NH3} (0~94%), IMEP ↑ 67%; P_{max} ↑ 10 bar/CAD	NO_x ↑ significantly with the T from 1400 K to 1800 K.	[97]
NH_3/H_2	H_2	• 4-cylinder • 4-stroke • direct injection	• CR = 15.3 • X_{NH3} (0~40%)	IMEP of mixture with NH_3 reached 3.1 bar, 1.2 times pure H_2.	NO_x (750 and 2000 ppm), N_2O ↑ under 1400 K.	[98]

↓ and ↑ are down and up respectively.

3.1.2. Combustion and Emission of NH_3/H_2 CI Engines

The higher CR and intake pressure work together to assist NH_3 combustion, reducing the required intake temperature, which is closely related to NO_x emissions, thereby maximizing IMEP and efficiency. However, strategies are needed to recover the loss of combustion efficiency and to avoid N_2O, which is prone to production below 1400 K [98]. To understand the feasibility of clean and efficient NH_3 combustion, the CR of the HCCI test stand was modified to 22:1, increasing IMEP by 67% with varying levels of X_{NH3} from 0 to 95%. However, when the P_{max} exceeds 10 bar/CAD, heat and friction losses sharply rise, ultimately limiting IMEP, indicating that NH_3 inhibits the overall combustion rate [97]. By adjusting the CR and injection time of the NH_3/H_2-fueled CI engines, NO_x emissions can be brought into compliance with Tier III emission standards while ensuring that the engine maintains sufficient power [61]. The best injection timing combination in the engine not only has optimum power and economy but also allows the engine's NO_x emissions to meet Tier II emission standards [99].

Building on these research results [61,99], Wang et al. [100,101] conducted a more detailed study on the influence of the NH_3/H_2 energy ratio on the pressure in the engine cylinder, power, and emissions. Mixing H_2 from 0 to 30% increased the cylinder explosion pressure by 10.7% and power by 1.8% while reducing the fuel consumption rate and NH_3 escape by 0.3% and 99.1%, respectively. Although NO_x emissions increased by 58.8%, the comprehensive performance of the CI engine after H_2 mixing combustion was improved. With the help of a small amount of diesel ignition, the engine adopted a direct injection method, and when using a mixture of NH_3 and H_2 as fuel, the optimal X_{H2} was found to be 30% [101]. Pathways to promote combustion and emission reduction in NH_3 CI engines as shown in Figure 13.
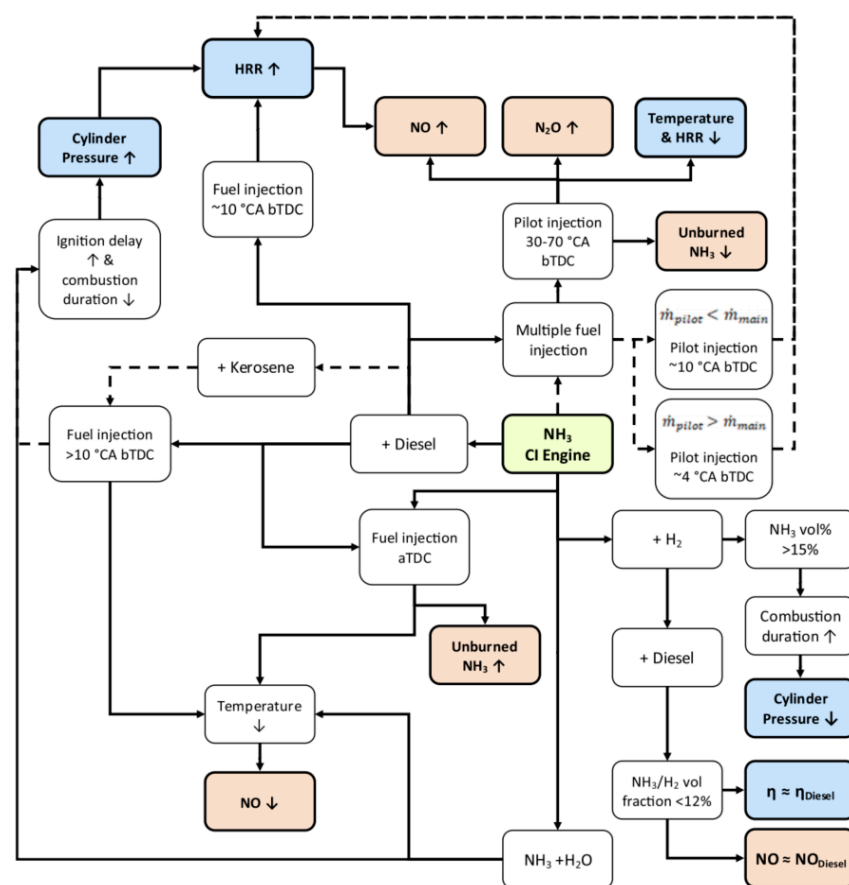
Figure 13. Pathways to promote combustion and emission reduction in NH_3 CI engines [102]. ↓ and ↑ are down and up respectively.

Due to the advantage of faster transmission speed that NH_3/H_2 combustion possesses and considering the convenience of energy transportation, NH_3 decomposition mixed with H_2 is an important measure to reduce the difficulty of H_2 storage and transportation. Gill et al. [103] conducted experiments to study the combustion and emission properties of various fuel types, including diesel, pure NH_3, pure H_2, $NH_3/H_2/N_2$ (1%, 75%, 24%), and $NH_3/H_2/N_2$ (2%, 75%, 23%). The results showed that incorporating more H_2 and NH_3 had a negative impact on BTE at both loads compared to pure diesel. At high loads, BTE with pure NH_3 was superior to BTE with added decomposition H_2, which was similar at low loads. Upon reducing the cylinder pressure from 5 bar to 3 bar, the total COV decreased by approximately 50%, BTE decreased by around 26%, and emissions of NO_x increased by about 27% [103].

3.1.3. Combustion and Emission of NH_3/DME CI Engines

Dimethyl ether (DME) shares physical properties with liquefied petroleum gas, featuring a high CN and low ignition temperature [104]. When mixed with other fuels, DME can enhance the combustion of low-activity fuels [105]. The addition of DME increases the reactivity of NH_3 and reduces ignition delay times, although this influence decreases with increasing DME, temperature, and pressure. This promotional effect is attributed to the increased formation rate and concentration of free radicals, especially OH [95].

Despite the inevitable increase in NO_x emissions due to the nitrogen bound in NH_3, improvements can be achieved under the same operating conditions by increasing the injection pressure. Using X_{NH3} (20% and 40%) results in an extended ignition delay time due to the elevated auto-ignition temperature and sluggish flame propagation speed, limiting the engine's load output. Higher NH_3 concentrations, coupled with higher injection pressures, can enhance the fuel–air mixture for better combustion and achieve a higher engine load output [106]. Given the high auto-ignition temperature of NH_3, the optimal injection time needs to be advanced with the increase in X_{NH3}. The suitable injection timing range for a DME/NH_3 blend (40%/60%) was determined to be 90 to 340 °CA before top dead center (BTDC). This advanced injection timing resulted in the engine displaying HCCI combustion characteristics [96]. Combustion and emission of NH_3 CI engines assisted by changing the structure and strategy as shown in Table 5.

Table 5. Combustion and emission of NH_3 CI engines assisted by changing the structure and strategy.

Test Fuel	Baseline	Power Equipment	Operating Conditions	Performance	Emissions	Ref.
NH_3/Algal biodiesel	Algal biodiesel	• 1-cylinder • 4-stroke	• CR = 17.5 • X_{NH3} (20%, 30%, 40%, and 50%) • load (20%, 40%, 60%, 80%, and 100%)	BTE were 34.1%, 35.4%, 36.7%, 33%, and 30.9% with different AEF.	NO_x ↓ 36.19%, 42.65%, 50.05%, and 52.64% with different AEF.	[54]
NH_3 (HTCGR)	diesel	• 6-cylinder • 2-stroke	• CR (20.5, 25, 50, 75) • load (100%)	Thermal efficiency can approach 50%, heat transfer loss is 3.4 times lower than in the original mode.	T ↑, P ↑, NO_x ↑	[81]
NH_3/H_2	NH_3/H_2	• 1-cylinder • 4-stroke • High-pressure common • direct injection	• CR (13.5 to 16.5) • injection timing from 12 to 24 (°CA BTDC) • NH_3/H_2 (7:3)	Delayed the injection timing, the ignition delay period ↓. CR increases by 1, hot zone appears 2 °CA ahead of time, and the area ↑.	At 12 °CA BTDC and CR = 13.5, the NO_x emissions suit Tier III.	[61]
NH_3/diesel (liquid)	NH_3/diesel (gaseous)	• 2-stroke • premixed combustion	• CR = 12 • 124 rpm • Pilot injection timing = −8 °CA ATDC	HRR ↑, P ↑; HRR ↑ 33%, 25%, P ↑ 11%, 18%, at 100% and 80% NH_3 energy supply, respectively.	NO_x emissions suit Tier II but not Tier III.	[83]
NH_3/diesel	diesel	• 1-cylinder • direct injection • 4-stroke • diesel pilot fuel	• CR = 17.7 • X_{NH3} (35%) • DEG = 33 °CA	Total efficiency ↓ 3.4%; 1.6 kW.	NO_x ↑ 7 times.	[107]

Table 5. *Cont.*

Test Fuel	Baseline	Power Equipment	Operating Conditions	Performance	Emissions	Ref.
NH_3/H_2	NH_3/H_2	• 2-stroke • pre-chambers • dual fuel injection	• CR = 12 • H_2 injection time (346 to 355 °CA) • spark ignition time (348.5 to 354.5 °CA)	Achieving the full-load power output.	NO_x emissions suit Tier III.	[108]
NH_3/DME	DME	• 1-cylinder • direct injection • 4-stroke • high-pressure common rail	• CR = 20 • engine speed (2200 to 3600 rpm)	Better combustion and higher workloads.	NO_x emissions at ppm level.	[106]
$NH_3/H_2/diesel$	NH_3/H_2	• 1-cylinder • 4-stroke • high-pressure common rail	• CR = 13.5 • 1800 rpm • load (100%) • the NH_3/H_2 mixing ratio is 7:3	P ↓ 5.71 MPa, engine power ↓ 2.59% under D708/A/H708.	NO_x emissions suit Tier III.	[99]

↓ and ↑ are down and up respectively.

3.2. Exhaust Gas Aftertreatment to Minimize NO$_x$ Emissions from CI Engines

To address the NO_x emission issue in NH_3-fueled CI engines, the use of NH_3 for the selective catalytic reduction (SCR) of NO_x is prevalent. For safety considerations, vehicle aqueous urea was injected into the aftertreatment device as an NH_3 carrier. However, the uneven distribution of aqueous urea can impact catalytic efficiency. In this context, researchers compared the impact of pressure-driven ejectors and air-assisted ejectors on the uneven distribution of aqueous urea [109]. The results indicate that air-assisted injection has clear advantages in both droplet size and injection speed. However, under the influence of airflow, aqueous urea is prone to solidify. In response, researchers designed I-type and L-type ejectors, influencing the amount and uniformity of NH_3 injection, respectively [110].

To enhance the mixing ratio of vehicle urea and exhaust gas and improve volume utilization, the influence of mixing chambers and swirl mixers with NO_x conversion was compared [111]. This comparison found that the NO_x conversion efficiency can be increased by 61.3%, 76.2%, and 86.3%, respectively, by using the mixing chamber, the swirl mixer, and a combination of the two [111]. Ko et al. [112] observed that NH_3 slip is inevitable in the process of NO_x conversion, especially during engine start, where it is challenging to eliminate NH_3 slip. However, Kuta et al. [92] discovered that NH_3 slip provides the possibility to re-activate the SCR system and improve its effectiveness under different engine operating conditions. The key factor affecting effectiveness is temperature, which can be easily controlled by modifying the structure of the exhaust device. SCR systems as shown in Figure 14.
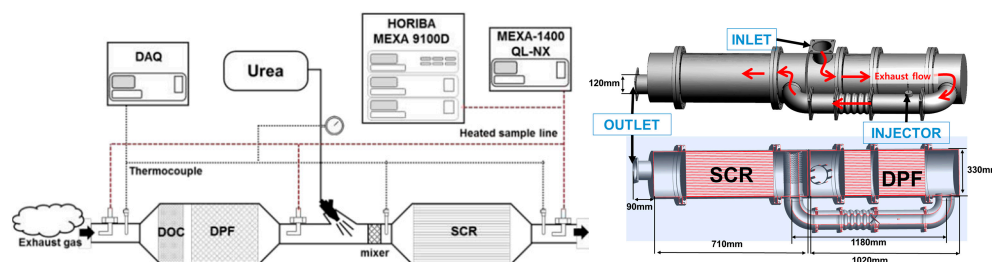
Figure 14. SCR systems [110,112].

4. Ammonia Used in Gas Turbines

The gas turbine (GT) is an internal combustion power machine that utilizes high-pressure air compressed by the compressor and fuel injected into the combustion chamber. The mixture of air and fuel ignites, creating high-temperature gas. Subsequently, this gas expands, driving the turbine to work externally. Combustion stability is achieved when the flame propagation speed matches the mixture flow velocity. The GT imposes strict requirements on fuel performance due to its high inlet flow rate, which is essential for maintaining stable combustion.

The combustion chamber of the GT exhibits distinctive features. These include high temperatures, elevated airflow velocity (leading to unstable flames that are prone to extinguishing, making combustion completion challenging), heightened combustion intensity (requiring a large fuel supply per unit volume and high combustion speed, necessitating a uniform outlet temperature field), and a high excess coefficient. The latter is particularly notable in areas of poor combustion, where working conditions are variable. These characteristics are illustrated in Figure 15.
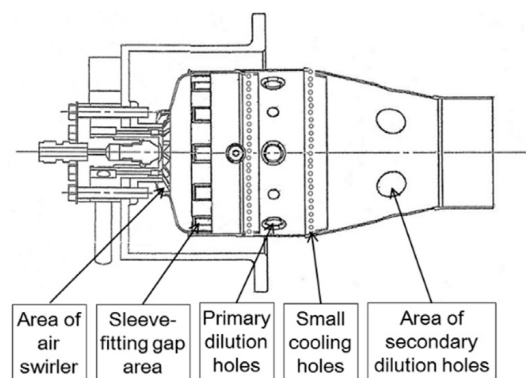
Figure 15. Schematic diagram of combustion chamber structure for GTs [113].

Verkamp et al. [114] experimentally studied the performance of the burner, minimum ignition energy, quenching distance, flame stability limit, and other physical properties of a NH_3/air mixture in a gas turbine burner. According to the existing combustion characteristics, it is predicted that pure NH_3 cannot be used as an alternative fuel for fueling GT power devices [115] unless the energy of the ignition system is increased and the injection strategy is optimized. To understand the NH_3 spray characteristics more comprehensively, Li et al. [115] established the relationship between superheat, fuel viscosity, temperature, ambient density, and NH_3 spray characteristics in a constant volume chamber. These experimental data will provide basic information for understanding NH_3 combustion. Based on the existing models of NH_3 sprays, An et al. [116] compared the simulation results with the recently published experimental data of NH_3 flash evaporation spray vaporization and discussed the effectiveness of the liquid NH_3 phase transition model concerning penetration length, diameter, and spray morphology. Through model evaluation, it was found that combining and optimizing multiple evaporation models to match the actual evaporation characteristics of liquid NH_3 would be an effective pathway.

4.1. Mixing Fuels with Strong Activity

4.1.1. Mixing NH_3 with CH_4

The low heat value and flame propagation speed of CH_4 are higher than those of NH_3. Adding CH_4 proves advantageous in enhancing the combustion efficiency of NH_3 [117]. Zhang et al. [118] discovered that incorporating CH_4 can broaden the ignition threshold of NH_3 flames. Additionally, the latent heat of CH_4 evaporation is lower than that of NH_3. The introduction of CH_4 helps mitigate the inhomogeneity of fuel droplets, reducing heat transfer and minimizing NO_x emissions and NH_3 slip [119]. Consequently, increasing the inlet temperature of CH_4/NH_3 mixed fuel and minimizing heat loss from the combustion chamber wall can compensate for fuel droplet spray-induced heat transfer losses. This improves droplet spray combustion characteristics and further reduces pollutant emissions [120]. The GT operated stably until X_{NH3} reached 63% [121]. Beyond 22% X_{NH3}, a noticeable drop in combustion efficiency and thermal efficiency occurred. A comparison between the NH_3 flame and the mixed fuel flame containing 10% CH_4, with different equivalence ratios, is illustrated in Figure 16.

For the multi-stage swirl combustor, an equivalence ratio of 1.2 is optimal for controlling minimum NO and NH_3 emissions [122]. However, for a single-stage swirl combustor,

the optimal equivalence ratio differs. Considering the relationship between NO_x emissions and unburned fuel, an equivalence ratio of 1.06 is optimal when X_{NH3} is 70% [123]. Irrespective of the NH_3 fraction, an equivalence ratio slightly greater than 1.05 is optimal for lower NO [124,125].
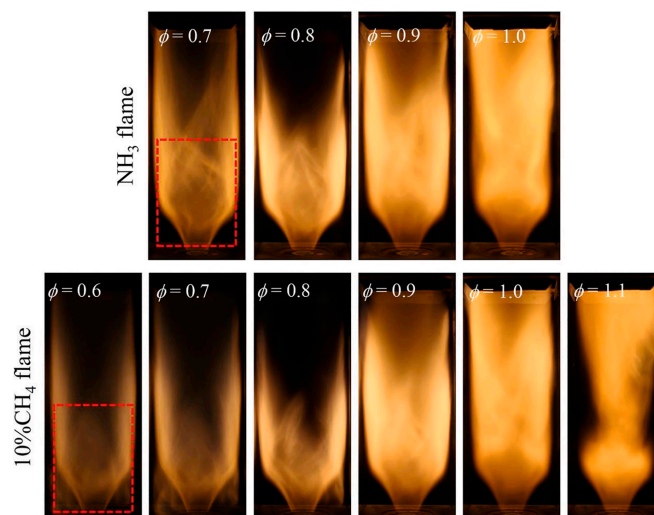
Figure 16. Comparison of the NH_3 flame and the mixed fuel flame containing 10% CH_4 with different equivalence ratios [126].

4.1.2. Mixing NH_3 with H_2

It has been demonstrated that the combustion intensity of NH_3/air can be enhanced by incorporating active fuels such as CH_4 and H_2. When a GT was fueled by NH_3/H_2/air and CH_4/air, it became evident that the GT fueled by NH_3/H_2/air exhibited superior performance, with a 37% higher efficiency. However, this improvement comes at the cost of unsatisfactory NO_x emissions. Zhang et al. [126] delved into the impact of CH_4 and H_2 on the emission characteristics of an NH_3-fueled GT burner. At an equivalence ratio of 0.1, whether it was NH_3/H_2, NH_3/CH_4, or NH_3 alone, the variations in NO and NO_2 were similar [126]. As the mixing ratio exceeded 0.1, owing to the higher combustion temperature, NH_3/CH_4 demonstrated notable performance in NO_x emissions. Utilizing the dynamic thickened flame model, it was verified that NH_3 co-fired with 10% H_2 is a promising mixture capable of enhancing combustion stability and maintaining NO_x emissions within a controllable threshold [127]. However, focusing on NO_x reduction alone results in lower efficiencies than CH_4, emphasizing the urgent need for new injection and ignition technologies to simultaneously reduce nitrogen oxides and unburned NH_3 emissions while maintaining power outputs [128]. Combustion techniques and combustor design for efficient combustion and low NO_x emission from an ammonia MGT swirl combustor are proposed, NO_x emission of 42 ppm was achieved [129]. Basic research parameters of a GT as shown in Figure 17.

To achieve high efficiency, fuel steam is directly introduced into the combustion chamber. Combined with other energy-saving technologies, this approach can achieve a total efficiency of 59%, while emissions still comply with European NO_x thresholds [130]. Lean premixed combustion technology, along with swirl-induced flame stabilization, represents one method for reducing NO_x emissions in traditional GTs. This method demonstrates that NO_x emissions remain below 30 ppm even when X_{NH3} reaches 40%, using air-staged combustion fueled by the NH_3/CH_4 mixture [131].
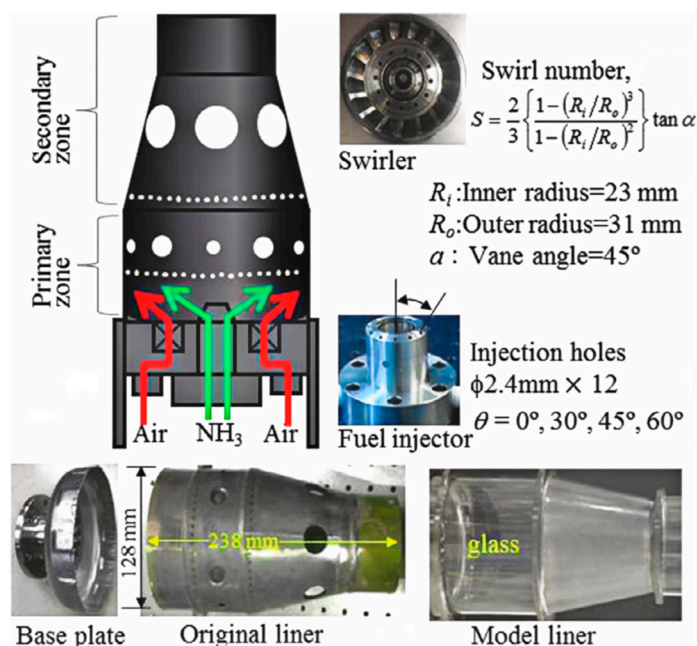
Figure 17. Basic research parameters of a GT [129].

In the pursuit of understanding the NO_x emission mechanism, researchers conducted studies on chemical kinetics models, incorporating actual NO_x emission tests to validate and refine the model parameters, ensuring the reliability of model simulation. Xiao et al. [132] compared five different chemical kinetics models to evaluate their accuracy in representing reaction dynamics in real GT burner conditions. These chemical kinetic models can simulate and predict the chemical pathway of CH_4 as an NH_3 combustion enhancer and the key reactions leading to NO_x emissions. Through the analysis of the chemical reaction pathway, it was observed that the addition of CH_4 promoted the formation of OH radicals, subsequently enhancing NH_3 conversion. Even in mixtures with lower NH_3 content, free radicals generated in the CH_4 oxidation pathway contributed to the formation of NO_x [133].

Various combustion mechanisms suggest that during NH_3/H_2 premixed combustion, NO is primarily reduced to NNH [134]. When burning the NH_3/H_2 mixture mixed with steam, the decomposition of H_2O promotes significant H, O, and OH radicals. While this hinders the formation of NO, the increased presence of OH radicals promotes the formation of NH_2, subsequently leading to the formation of NO [135]. These findings have been confirmed in [128] on NH_3/H_2 lean premixed combustion in a swirl GT combustor. The change in NO_x emissions aligns with the concentration pattern of OH radicals in the combustion chamber, underscoring the significance of OH radicals in fuel NO_x [136]. The increase in pressure enhances the reaction of $NH + NO = N_2O + H$, with higher pressure resulting in a lower NO fraction [137].

With a 40% increase in NH_3 addition, the OH concentration consistently follows the temperature trend [138]. Analyzing the NO reaction pathway influenced by temperature reveals that the main factor affecting NO formation in the flame zone is HNO free radicals, while the primary factor influencing NO reduction in the post-flame zone is NHi free radicals [138]. The addition of H_2 increases the concentrations of H, NH, and NH_2 at the flame root, leading to increased NO consumption [127].

4.2. Structure Adjustment and Auxiliary Combustion Measures

Due to the significant advantages of plasma in enhancing the NH_3 decomposition rate and laminar combustion rate, as illustrated in Figure 18, plasma-assisted combustion strategies are extensively employed in GT ignition systems [139]. Scientists utilize nanosec-

ond plasma discharge to increase pulse energy density and have observed that the flame combustion rate (X_{H2} = 12%) remains consistent with conventional fuel [133].
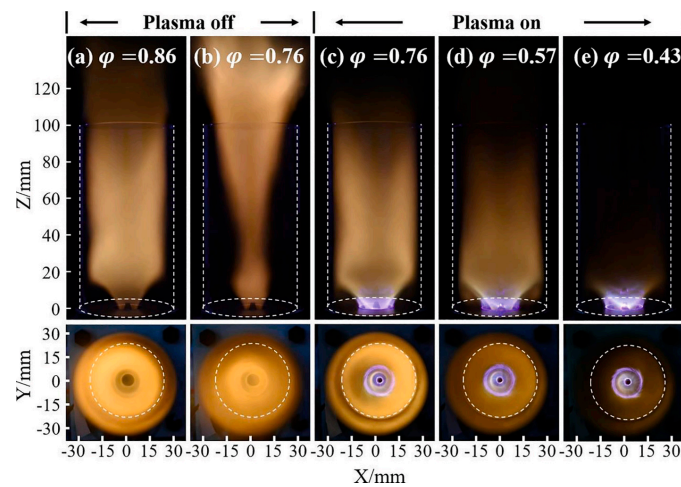
Figure 18. The effects of plasma on a swirling NH_3 flame [41,139].

To effectively reduce NO_x emissions, it is recommended to employ the non-premixed injection mode and maintain an equivalence ratio of 0.9 to 1.2 when operating with a higher proportion of NH_3 in the fuel mixture [140]. Kurata et al. [113] successfully developed a non-premixed combustion chamber suitable for NH_3 combustion with low NO_x emissions, capable of achieving a power output of up to 40 kW under pure NH_3 combustion conditions, effectively demonstrating the potential of NH_3 combustion to achieve dual carbon targets [141]. The lower swirl combustion burner exhibited a wider uniform reaction area, fewer hot spots in the reaction zone, and a more uniform temperature distribution. The maximum NO_x concentration in the reaction zone with the higher swirl combustion burner was twice that of the lower swirl combustion burner [142].

Although a larger equivalence ratio contributes to lower NO_x emissions, it also compromises the overall efficiency of the GT. Okafor et al. [121] determined that the optimal primary combustion zone for low NO_x emissions corresponds to an equivalence ratio ranging from 1.30 to 1.35, depending on the ammonia mole fraction (X_{NH3}). Lean-rich combustion of CH_4/NH_3 mixtures yielded lower NO_x emissions compared to pure NH_3 combustion due to the faster flame speed of CH_4/NH_3 mixtures, which reduced NO_x formation in the secondary combustion zone [121]. Somarathne et al. [119] conducted a comparative analysis of combustion and emission characteristics of pure NH_3 and CH_4 in a combustor designed for a rich-lean GT. NO concentration was primarily influenced by local temperature. While cooling the combustor wall considerably impacted NH_3 oxidation and NH_3 slip, it also reduced NO emissions by lowering the concentration of OH radicals in the flame zone due to wall heat losses [119]. Lean premixed flames, a promising technique for hydrocarbon combustion, effectively comply with strict legislative regulations on emissions of combustion pollutants in GT combustion but lead to combustion instability. Lean-rich combustion systems can achieve minimal NO levels while producing zero unburnt NH_3 emissions [113]. NO_x emissions are significantly influenced by the mixture stoichiometry [143]. Moreover, with increasing X_{NH3}, the decrease in NO_x emissions becomes more pronounced as the equivalence ratio increases [129]. In summary, Figure 19 illustrates the technical approach for improving the combustion and emission performance of NH_3-fueled GTs. NO_x emissions and NH_3 slip can be effectively reduced by optimizing the structure and strategy and incorporating auxiliary combustion measures. While blending highly active fuels can improve thermal efficiency, it is relatively easy to increase NO_x emissions.
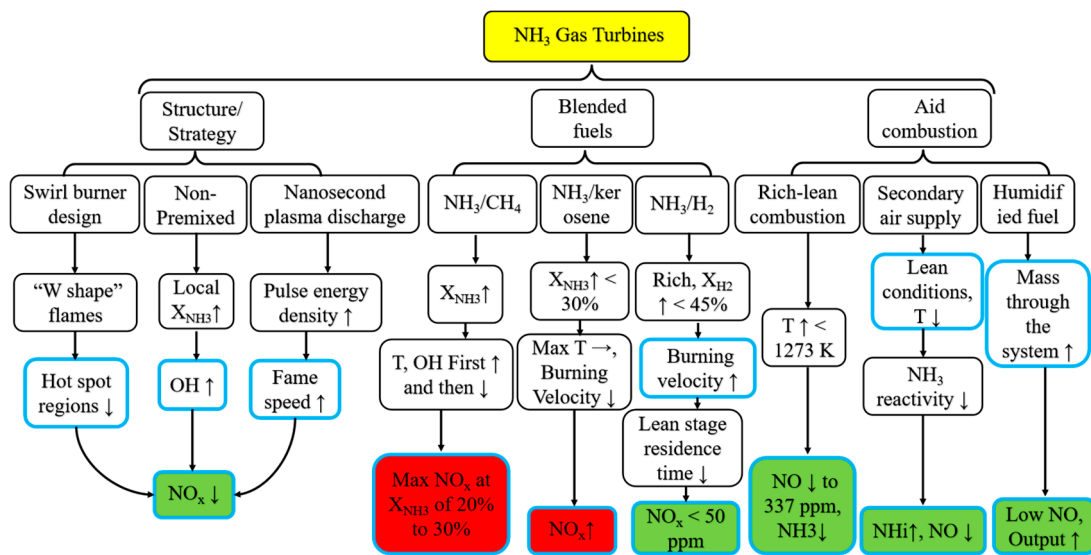
Figure 19. Pathways to promote combustion and emission reduction in NH$_3$ GTs. ↓, ↑, → are down, up, unchanged respectively.

5. NH$_3$ Fuel Cells

5.1. Application of NH$_3$ in FCs

The breakthrough in the research and development of NH$_3$ FCs can be attributed to the large-scale production of fuel, application processes that significantly reduce carbon emissions, and other advantages [10,144]. NH$_3$ FCs are classified based on different types of fuel supply and electrolytes [145], as illustrated in Figure 20. In the pursuit of higher power density, scholars have conducted studies on factors influencing the performance of NH$_3$ FCs, including reaction temperature, electrolyte thickness, electrolyte type, and electrode type. The research results on the performance of NH$_3$ FCs are combined, and different power segments are depicted, in Figure 21 [146].

According to Figure 21, the solid oxide fuel cell (SOFC) fueled with NH$_3$ demonstrates superior power output compared to the alkaline electrolyte fuel cell (AEFC). The highest power density reported for AEFC in [142] is only 467 mW/cm^2, and the volume power density is a mere 8 kW/m^3 [147].

Indirect ammonia FCs (IA-FCs) utilize H$_2$ derived from the thermal decomposition of NH$_3$ as fuel, offering a wider range of applications. Researchers have conducted preliminary studies on the performance of IA-FCs [147]. Although indirect ammonia–proton exchange membrane fuel cells (IA-PEMFC) exhibit slightly lower efficiency, they boast remarkable power density, with a volume power density approximately 15.5 times that of IA-AEFCs and 12.2 times that of SOFCs fueled with NH$_3$ [146].
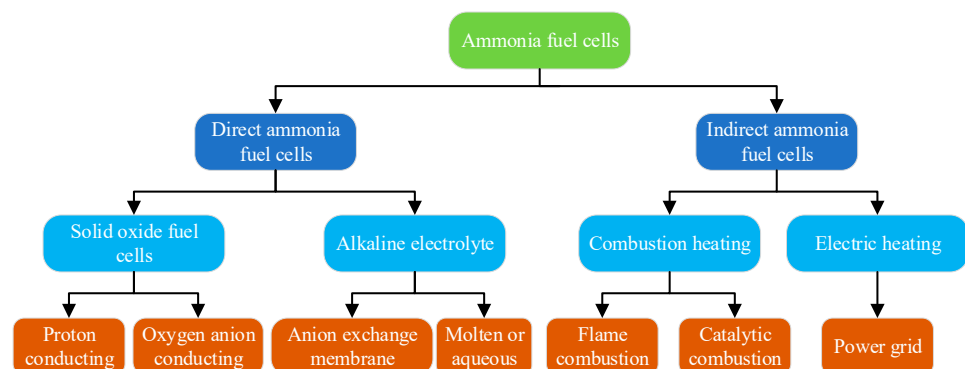
Figure 20. Classification of NH$_3$ FCs.
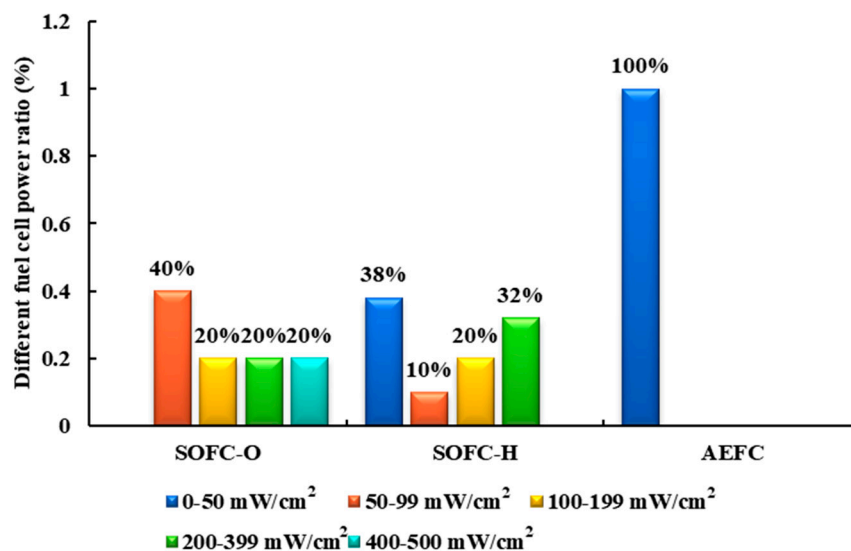
Figure 21. Power interval distribution of direct NH$_3$ FCs.

5.2. Research Routes of IA-PEMFCs

Research on IA-PEMFCs is progressively deepening, with three main research routes. Firstly, the issue of heat supply through electric heating emerges as a stable and easily adjustable heating technique [148]. However, the use of the end product, electricity, may inevitably reduce the overall power generation efficiency for FCs [149]. This method is primarily employed to provide a stable heat source for verifying the effectiveness of catalysts (such as zeolite-based [150], Mo2N [151], Ru-Al monoliths [152], nickel-based [153], and Ce-doped [154]) and other improvement measures for FCs [153]. Catalytic combustion, a flameless combustion mode, offers advantages such as high combustion efficiency, a stable and controllable process, and relatively uniform and stable combustion. The catalytic combustion heating mode can decompose NH$_3$ to form an ideal exothermic and endothermic coupling system with high volume utilization efficiency. Currently, NH$_3$ catalytic combustion is primarily utilized in power equipment with small power and strict volume requirements. Ongoing research focuses on catalysts to enhance catalytic combustion efficiency (including Mn/Bi/Al catalysts [155], platinum [156], Ru/Al$_2$O$_3$ [157], and Pt gauzes/oxide monolithic layers [158]) and reactor structure [159]. Flame combustion, on the other hand, is a simple, direct, and rough heating method with high combustion temperature but low combustion efficiency. Current research on NH$_3$ flame combustion primarily concentrates on the stability of NH$_3$ combustion (including pure NH$_3$ combustion [55,160,161], mixed combustion [162–164], and auxiliary combustion [31,165]) and reducing NO$_x$ emissions [166–169]. The chemical reaction process in direct NH$_3$ FCs and IA-PEMFCs is illustrated in Figure 22.

The second research route involves purifying the gas resulting from NH$_3$ decomposition. In an ideal state, the gas would be a 1:3 mixture of N$_2$ and H$_2$. However, achieving a 100% NH$_3$ decomposition rate is highly unlikely, and the gas will inevitably contain some undecomposed NH$_3$. Additionally, NH$_3$ decomposition gas contains 25% N$_2$, and the presence of N$_2$ is ineffective, further reducing the mass transfer effect [170,171]. However, PEMFCs are highly sensitive to NH$_3$ content, which needs to be below 0.1 ppm for optimal performance [172]. Therefore, to improve the service life and power generation efficiency of subsequent FCs, the purification of NH$_3$ decomposition gas is of great significance [173]. Currently, the purification of NH$_3$ decomposition gas is primarily studied in H$_2$-selective membranes [174], membrane reactors [175–177], and the liquefaction of N$_2$ [178].
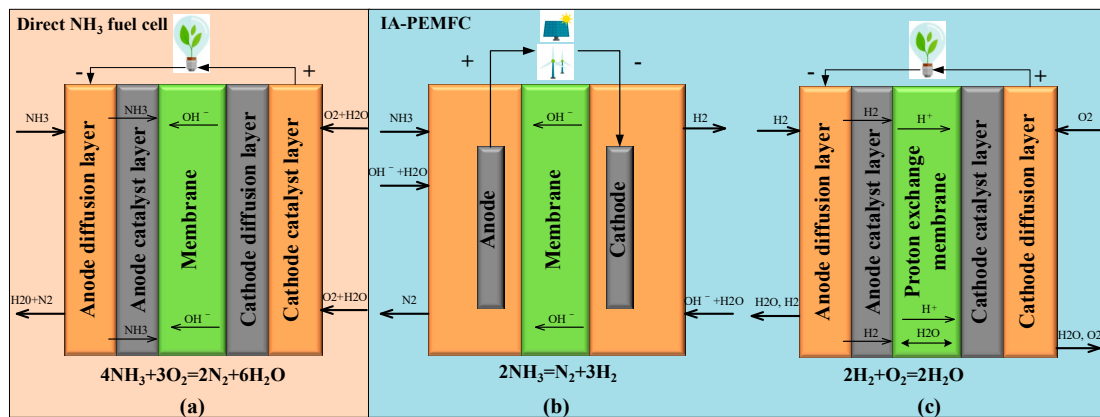
Figure 22. Chemical reaction process in direct NH_3 FCs (**a**) and IA-PEMFCs ((**b**) NH_3 decomposition, (**c**) PEMFC).

The third research route involves developing a FC structure suitable for the mixture of N_2 and H_2. Zhao et al. [179] demonstrated through experiments that it was challenging for an air-cooled H_2–air PEMFC to function properly when an N_2 and H_2 mixture was used as the anode fuel. Subsequent research by Zhao et al. [180] indicated that shortening the flow channel length could enhance the stability of PEMFCs using a N_2 and H_2 mixture as fuel, as revealed through simulation analysis. Building on this work, Hu et al. [181] further investigated the water–heat–gas distribution of NH_3/H_2 PEMFCs under parallel flow channels. They found that fuel dead zones tended to appear at the tail of long parallel flow channels, impacting the normal operation of the FC. Considering the mass transfer characteristics of the N_2/H_2 mixture, Hu et al. [147] employed biomimicry to construct a hedge-type triangular flow channel, optimizing it for N_2/H_2 mixture compatibility and determining size parameters for optimal output performance. These studies demonstrate that, by employing flow channel optimization and other measures, NH_3 decomposition gas can be directly injected into PEMFCs after removing NH_3, resulting in higher power density than conventional FCs.

Hunter et al. [182] explored the system efficiency of IA-PEMFCs by integrating an NH_3 cracking system, a purification unit, and a small PEMFC. The integration of a complete system for NH_3 decomposition and NH_3 decomposition gas purification, based on light metal amide imide with a 100 W PEMFC, is a significant milestone for the promotion and application of indirect NH_3 FCs. Ye et al. [148] used the heating method of NH_3/H_2 mixed flame combustion to heat NH_3 decomposition gas and added a NO_x emission reduction treatment device to analyze the fuel utilization efficiency of the indirect NH_3 FC system. Compared with conventional fuel-oil engines, the fuel utilization efficiency of the IA-PEMFC system is higher than that of water taxis but lower than cargo ships [148]. Lin et al. [183] categorized the heat sources needed for NH_3 decomposition in the IA-PEMFC system into three heating modes: electric heating, N_2/H_2 flame combustion, and PEMFC anode tail gas combustion. They then compared and analyzed the system efficiency under each mode. Among them, the IA-PEMFC system, where the combustion of NH_3 decomposition gas provided heat for NH_3 decomposition, had the highest efficiency, accounting for 56.6%. Building on the IA-PEMFC system, Zhao et al. [184] established a complete system that burned the anode tail gas of PEMFC to supply the heat required by the decomposer. When the heat from firing the anode tail gas is insufficient, fueling the NH_3 gas to supply the required heat to the decomposer becomes a compensatory strategy. The system's energy efficiency is found to be 45% through simulation analysis.

The optimization results of system efficiency in the IA-PEMFC system above are inevitably different, as shown in Figure 23, due to the varying catalyst activity, catalyst dose, regenerator efficiency, and other parameters used in the experiment and simulation.

However, the successful integration of the IA-PEMFC system above fully demonstrates the feasibility of the system. This paves the way for the future advancement of IA-PEMFCs.
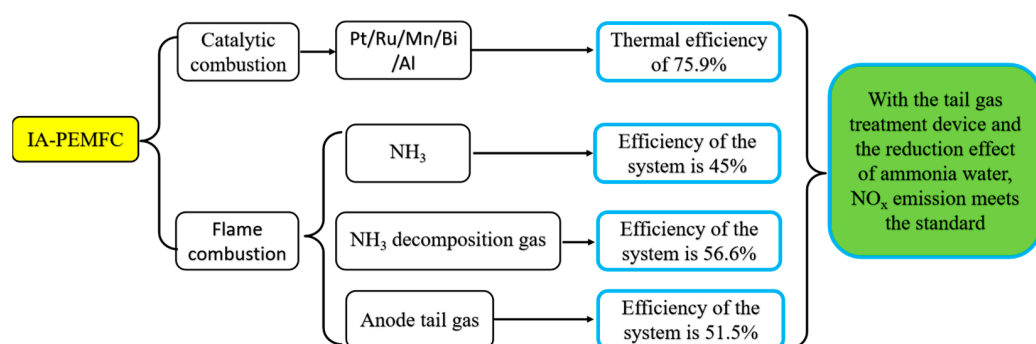
Figure 23. Research routes of IA-PEMFCs.

5.3. NO$_x$ Emission and NH$_3$ Slip in IA-PEMFCs

NH$_3$, while not classified as a greenhouse gas, is considered toxic. Therefore, NH$_3$ slip serves as an indicator of harmful emissions. NH$_3$ slip primarily occurs in direct NH$_3$ FCs and can be mitigated by factors such as purge strategy optimization of the flow channel structure, catalyst selection, or operating conditions. Additionally, water generation at the anode aids in NH$_3$ absorption. Indirect NH$_3$ FCs primarily emit NO$_x$, mainly due to intermediate products generated by catalytic and flame combustion. Unlike GTs, which have a turbulent swirl parameter design, SI engines, which involve ignition time and flame diffusion combustion, or CI engines, which involve ignition time and premix combustion, NH$_3$ flame combustion in IA-PEMFCs focuses primarily on flame stability. The relatively stable combustion environment and simple, controllable flame combustion in IA-PEMFCs necessitate NO$_x$ emission reduction measures distinct from those employed in other power equipment. Typically, slightly richer combustion conditions [185] or higher initial pressure [186] can effectively suppress NO$_x$ production in NH$_3$-fueled combustion systems. Adding H$_2$ can significantly enhance NH$_3$ fuel combustion speed and improve the HRR to meet the heat requirement for NH$_3$ decomposition [187]. However, the addition of H$_2$ also leads to increased NO$_x$ emissions. Therefore, further research is warranted to investigate the interaction between NH$_3$ and NO in the reduction region under humidification conditions [188]. The reaction of O + H$_2$O = 2 OH reduces the concentration of O free radicals, limiting the reaction rate of N$_2$ + O = NO + N [189]. Plasma ignition can effectively control NO$_x$ emissions while enhancing combustion intensity. This is attributed to the ability of plasma ignition to generate OH radicals, reduce flame stagnant time, hinder the NO$_x$ generation pathway, and accelerate the rate of NH$_3$ combustion, directly generating N$_2$ [190].

Under ideal conditions, the products of NH$_3$ catalytic combustion are nitrogen and water. However, other reaction pathways may occur in the actual catalytic oxidation process, leading to the generation of NO$_x$ and NH$_3$ slip. Wickham et al. [191] developed a selective catalyst combined with surface oxygen atom adsorption treatment technology, promoting the efficient and selective decomposition of NH$_3$ into N$_2$ and water. Noskov et al. [155] found that the Mn/Bi/Al catalyst exhibited a high selectivity to NO$_x$, reaching up to 88% in a fluidized bed reactor test. In an oxygen/steam environment, Warner et al. [156] investigated 95% Pt/5% Rh gauze. Based on the influence of temperature and equivalence ratio on NO$_x$ formation, a selective formation mechanism model of NO$_x$ in the catalytic oxidation process of NH$_3$ was established. This model provides a pathway for the selective formation of NO$_x$ in later catalytic oxidation processes [156,158]. To reduce NO$_x$ emissions, lowering the reactor temperature, utilizing N$_2$ selective catalysts (such as Pt/Al$_2$O$_3$), or employing SCR technology are considered effective measures [192].

6. NO$_x$ Generation Mechanism Related to Ammonia Combustion

The mechanism of NO$_x$ formation during ammonia oxidation under low- and high-temperature conditions is shown in Figure 24 (left). Compared to low-temperature conditions, under high-temperature conditions, NH$_2$ generates a new product, NH, under the action of OH radicals, which are reduced to NO through O$_2$. At the same time, the new intermediate product H$_2$NH increases the pathway of NO$_2$ generation [193]. The changes in ammonia oxidation under different air/fuel ratios at the same temperature are shown in Figure 24 (right). The air/fuel ratio only affects the conversion rate of various products and does not affect the types of products produced during the ammonia oxidation process. From Figure 24 (right)., the air/fuel ratio is increased to 0.9, and the most significant factors affecting the conversion rate are NNH→HNO, NH$_2$→HNO, and NO→NO$_2$, which in turn affect the amount of NO$_x$ generated.
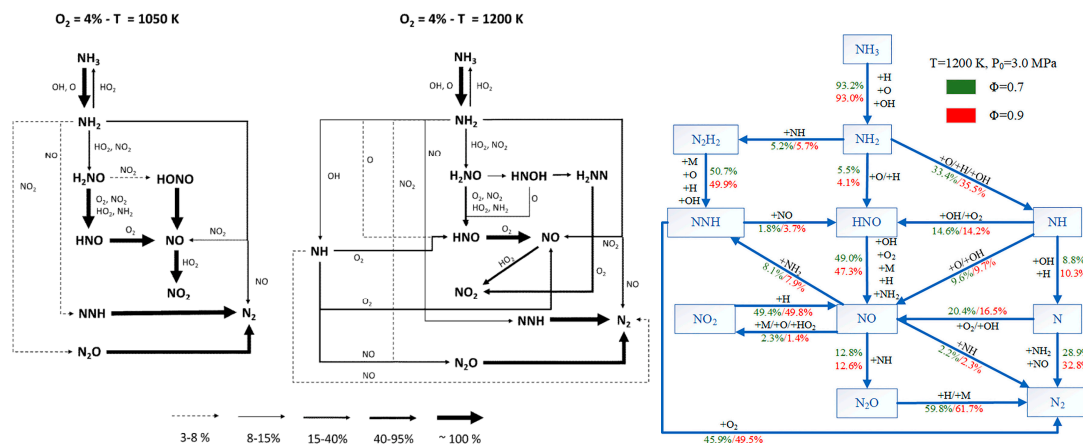
Figure 24. The pathway of NO$_x$ formation under the influence of temperature with an equivalent air/fuel ratio (**left**); under the influence of the air/fuel ratio with equivalent pressure (**right**) [193,194].

Figure 25 shows the simulation results of the ammonia oxidation process, producing NO through two commonly used reaction mechanisms, Mei and CEU-NH$_3$, under different combustion pressures. It can be seen from the figure that different reaction mechanism models correspond to different ammonia oxidation processes. In addition, all reactions involved in the oxidation of ammonia to NO gradually strengthen with the increase in combustion pressure, and the effect is significant.
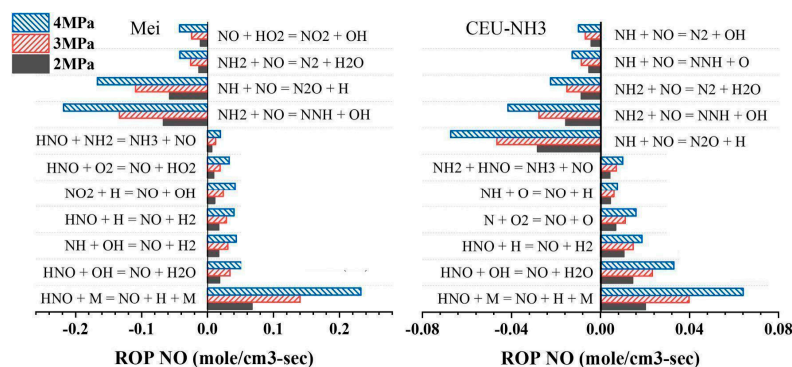
Figure 25. NO formation pathways under the influence of combustion pressure for different mechanism models [36].

When burning an ammonia–hydrogen mixture, the mechanism of NO$_x$ generation with different energy ratios is shown in Figure 26. Changing the energy ratio of the mixed fuel not only affects the types of intermediate products but also affects the reaction pathways

of different reactants. Among them, the newly added reactions are R178, R127, R173, R103, R123, R51, R50, and R105, and the more sensitive reactions were R20, R29, R53, and R49. When methane, DME, and traditional fuel are mixed with ammonia, their own products do not participate in the ammonia oxidation process. Therefore, when these fuels are mixed with ammonia, the actual influence is the ammonia oxidation reaction temperature and combustion chamber pressure, air/fuel ratio, energy ratio, etc. The influence of these factors on ammonia oxidation has been described above.
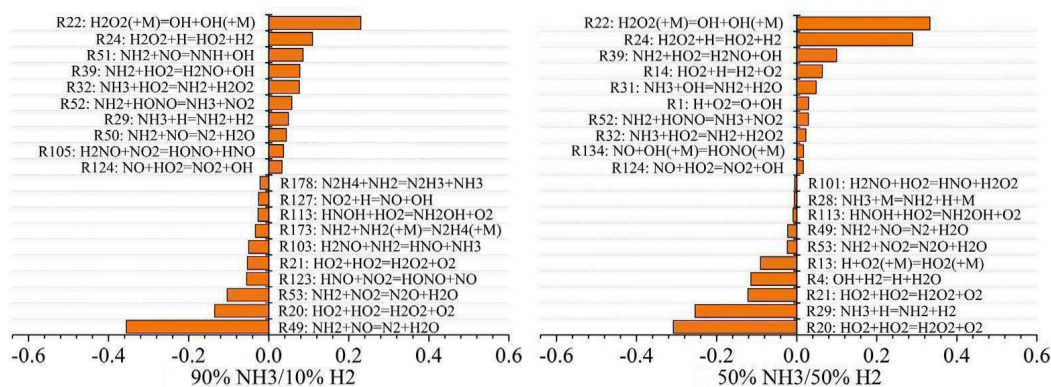
Figure 26. The formation mechanism of NO_x when burning an ammonia–hydrogen mixture with different energy ratios [195].

7. Conclusions

Based on the difference in the structure and working principle of different power equipment, this paper delves into the combustion and NO_x emission characteristics of NH_3 fuel in various power equipment, including SI, CI, and GT, from the perspectives of mixed fuel types and modes, structural design and operating strategies, and auxiliary combustion techniques. It also summarizes the current status of NH_3-FC applications and elaborates on the different heat sources and NO_x emissions associated with IA-PEMFCs.

With the comprehensive combination of mixed fuel, structural adjustment, auxiliary combustion, and other technologies, NH_3 fuel can burn stably in ICE, and the power and NO_x emissions are within the acceptable range. In addition to NH_3/H_2, NH_3/CH_4 and its mixture with gasoline can also be used in SI, NH_3/DME and its mixture with diesel can also be used in CI, and NH_3/CH_4 and its mixture with kerosene can also be used in GT. Compared with CI, when SI uses a NH_3/H_2 mixture for combustion, due to the controllable CR and ignition energy, the amount of NH_3 can be added in a wide range, while when NH_3/H_2 is used in GTs for combustion, the amount of NH_3 added is not more than 55%. In addition, beyond 22% X_{NH_3}, a noticeable drop in combustion efficiency and thermal efficiency occurred, while the GT operated stably until X_{NH_3} reached 63%.

Due to the high autogenous ignition temperature of NH_3 fuel and the structural differences between SI and CI, the allowable CR of SI and CI are not more than 15 and 21.9, respectively. In addition, the combustion characteristics of NH_3 fuel in SI can be improved by supercharging, increasing CR, prolonging ignition time, increasing the number of spark plugs, and other structure adjustment technologies, as well as the use of EGR, preheating, NH_3 cracking, and other auxiliary combustion technologies. CI uses multiple fuel strategies and split diesel injection, while GT generally adopts structural strategies such as optimizing cyclones, non-premixed combustion, plasma discharge devices, and auxiliary combustion technologies such as rich lean combustion and secondary air supply.

Compared with DAFC systems, IAFC is the best option for train powertrains when considering storage space and fuel costs, but the high technology requirements of the purifier pose a challenge. Benefiting from the operating high temperature of DAFC, reducing the NH_3 cracker and purifier of DAFC systems is still at the lab level.

Emission reduction technologies are mainly divided into SCR technology, staged combustion technology, and medium–low oxygen combustion technology. The research

on SCR Technology is that the chemical adsorption of functional groups on the surface of carbon-based materials should be further studied due to the influence of other pollutants.

Conflicts of Interest: The authors declare no conflict of interest.

References

1. WMO. *Provisional State of the Global Climate in 2022*; WMO: Geneva, Switzerland, 2022; Volume 26.
2. International Renewable Energy Agency (IRENA). *World Energy Transitions Outlook 2022*; International Renewable Energy Agency: Abu Dhabi, United Arab Emirates, 2022.
3. International Energy Agency. *Net Zero by 2050: A Roadmap for the Global Energy Sector 2021*; International Energy Agency: Paris, France, 2021; Volume 70.
4. United Nations. *SDGs Report 2023*; United Nations: New York, NY, USA, 2023.
5. Barnett, H. The European court of justice. In *Constitutional & Administrative Law*, 5th ed.; Routledge: London, UK, 2004. [CrossRef]
6. IPCC. *Strengthening and Implementing the Global Response*; IPCC: Geneva, Switzerland, 2022. [CrossRef]
7. IPCC. *Impacts of 1.5 °C Global Warming on Natural and Human Systems*; IPCC: Geneva, Switzerland, 2022. [CrossRef]
8. Solomon, B.D. Energy carriers. In *Dictionary of Ecological Economics: Terms for the New Millennium*; Edward Elgar Publishing: Cheltenham, UK, 2023; p. 185. [CrossRef]
9. Luo, Y.; Shi, Y.; Cai, N. *Ammonia: A Clean and Efficient Energy Carrier for Distributed Hybrid System*; Elsevier Inc.: Amsterdam, The Netherlands, 2021. [CrossRef]
10. Lewis, J. *Fuels without Carbon: Prospects and the Pathway Forward for Zero-Carbon Hydrogen and Ammonia Fuel*; Ammonia Energy Association: Ashburn, VA, USA, 2018.
11. Zamfirescu, C.; Dincer, I. Using ammonia as a sustainable fuel. *J. Power Sources* **2008**, *185*, 459–465. [CrossRef]
12. By, I.; Vassiliadou, E.; Amirkhanian, S.N. *Renewable Ammonia Generation, Transport, and Utilization in the Transportation Sector*; Ammonia Energy Association: Ashburn, VA, USA, 2019; Volume 11, pp. 295–301.
13. Faye, O.; Szpunar, J.; Eduok, U. A critical review on the current technologies for the generation, storage, and transportation of hydrogen. *Int. J. Hydrogen Energy* **2022**, *47*, 13771–13802. [CrossRef]
14. Ezzat, M.F.; Dincer, I. Comparative assessments of two integrated systems with/without fuel cells utilizing liquefied ammonia as a fuel for vehicular applications. *Int. J. Hydrogen Energy* **2018**, *43*, 4597–4608. [CrossRef]
15. Cui, J.; Aziz, M. Techno-economic analysis of hydrogen transportation infrastructure using ammonia and methanol. *Int. J. Hydrogen Energy* **2023**, *48*, 15737–15747. [CrossRef]
16. Wang, W.; Herreros, J.M.; Tsolakis, A.; York, A.P.E. Ammonia as hydrogen carrier for transportation; Investigation of the ammonia exhaust gas fuel reforming. *Int. J. Hydrogen Energy* **2013**, *38*, 9907–9917. [CrossRef]
17. Bartels, J.R. *A Feasibility Study of Implementing an Ammonia Economy*; Iowa State University: Ames, IA, USA, 2008; Volume 102.
18. De Vries, N.; Okafor, E.C.; Gutesa-Bozo, M.; Xiao, H.; Valera-Medina, A. *Use of Ammonia for Heat, Power and Propulsion*; Elsevier Inc.: Amsterdam, The Netherlands, 2020. [CrossRef]
19. Berwal, P.; Kumar, S.; Khandelwal, B. A comprehensive review on synthesis, chemical kinetics, and practical application of ammonia as future fuel for combustion. *J. Energy Inst.* **2021**, *99*, 273–298. [CrossRef]
20. Olabi, A.; Abdelkareem, M.A.; Al-Murisi, M.; Shehata, N.; Alami, A.H.; Radwan, A.; Wilberforce, T.; Chae, K.-J.; Sayed, E.T. Recent progress in Green Ammonia: Production, applications, assessment; barriers, and its role in achieving the sustainable development goals. *Energy Convers. Manag.* **2023**, *277*, 116594. [CrossRef]
21. MacFarlane, D.R.; Cherepanov, P.V.; Choi, J.; Suryanto, B.H.; Hodgetts, R.Y.; Bakker, J.M.; Vallana, F.M.F.; Simonov, A.N. A Roadmap to the Ammonia Economy. *Joule* **2020**, *4*, 1186–1205. [CrossRef]
22. Valera-Medina, A.; Xiao, H.; Owen-Jones, M.; David, W.I.F.; Bowen, P.J. Ammonia for power. *Prog. Energy Combust. Sci.* **2018**, *69*, 63–102. [CrossRef]
23. Egerer, J.; Grimm, V.; Niazmand, K.; Runge, P. The economics of global green ammonia trade "Shipping Australian wind and sunshine to Germany". *Appl. Energy* **2023**, *334*, 120662. [CrossRef]
24. Krishnamoorthi, M.; Malayalamurthi, R.; He, Z.; Kandasamy, S. A review on low temperature combustion engines: Performance, combustion and emission characteristics. *Renew. Sustain. Energy Rev.* **2019**, *116*, 109404. [CrossRef]
25. Viggiano, A.; Magi, V. *A Comprehensive Perspective on a Promising Fuel for Thermal Engines: Syngas and Its Surrogates*; Elsevier Inc.: Amsterdam, The Netherlands, 2023. [CrossRef]

26. Morlanés, N.; Katikaneni, S.P.; Paglieri, S.N.; Harale, A.; Solami, B.; Sarathy, S.M.; Gascon, J. A technological roadmap to the ammonia energy economy: Current state and missing technologies. *Chem. Eng. J.* **2021**, *408*, 127310. [CrossRef]

27. Cornelius, W.; Huellmantel, L.W.; Mitchell, H.R. *Ammonia as an Engine Fuel*; SAE Technical Paper; SAE International: Warrendale, PA, USA, 1965. [CrossRef]

28. Starkman, E.S.; James, G.E.; Newhall, H.K. *Ammonia as a Diesel Engine Fuel: Theory and Application*; SAE Technical Paper; SAE International: Warrendale, PA, USA, 1967. [CrossRef]

29. Starkman, E.S.; Samuelsen, G.S. Flame-propagation rates in ammonia-air combustion at high pressure. *Symp. Combust.* **1967**, *11*, 1037–1045. [CrossRef]

30. Liu, Z.; Zhou, L.; Zhong, L.; Wei, H. Enhanced combustion of ammonia engine based on novel air-assisted pre-chamber turbulent jet ignition. *Energy Convers. Manag.* **2023**, *276*, 116526. [CrossRef]

31. Grannell, S. The Operating Features of a Stoichiometric, Ammonia and Gasoline Dual Fueled Spark Ignition Engine. Ph.D. Thesis, University of Michigan, Ann Arbor, MI, USA, 2008.

32. Wu, Y.; Zhang, Y.; Xia, C.; Chinnathambi, A.; Nasif, O.; Gavurová, B.; Sekar, M.; Anderson, A.; Chi, N.T.L.; Pugazhendhi, A. Assessing the effects of ammonia (NH₃) as the secondary fuel on the combustion and emission characteristics with nano-additives. *Fuel* **2023**, *336*, 126831. [CrossRef]

33. Li, T.; Duan, Y.; Wang, Y.; Zhou, M.; Duan, L. Research progress of ammonia combustion toward low carbon energy. *Fuel Process. Technol.* **2023**, *248*, 107821. [CrossRef]

34. Li, H.; Xiao, H.; Sun, J. Laminar burning velocity, Markstein length, and cellular instability of spherically propagating NH₃/H₂/Air premixed flames at moderate pressures. *Combust. Flame* **2022**, *241*, 112079. [CrossRef]

35. Cai, T.; Zhao, D.; Gutmark, E. Overview of fundamental kinetic mechanisms and emission mitigation in ammonia combustion. *Chem. Eng. J.* **2023**, *458*, 141391. [CrossRef]

36. Liu, S.; Lin, Z.; Zhang, H.; Lei, N.; Qi, Y.; Wang, Z. Impact of ammonia addition on knock resistance and combustion performance in a gasoline engine with high compression ratio. *Energy* **2023**, *262*, 125458. [CrossRef]

37. Westlye, F.R.; Ivarsson, A.; Schramm, J. Experimental investigation of nitrogen based emissions from an ammonia fueled SI-engine. *Fuel* **2013**, *111*, 239–247. [CrossRef]

38. Kurien, C.; Mittal, M. Review on the production and utilization of green ammonia as an alternate fuel in dual-fuel compression ignition engines. *Energy Convers. Manag.* **2022**, *251*, 114990. [CrossRef]

39. Wei, W.; Li, G.; Zhang, Z.; Long, Y.; Zhang, H.; Huang, Y.; Zhou, M.; Wei, Y. Effects of ammonia addition on the performance and emissions for a spark-ignition marine natural gas engine. *Energy* **2023**, *272*, 127092. [CrossRef]

40. Zhang, R.; Chen, L.; Wei, H.; Li, J.; Chen, R.; Pan, J. Understanding the difference in combustion and flame propagation characteristics between ammonia and methane using an optical SI engine. *Fuel* **2022**, *324*, 124794. [CrossRef]

41. Elbaz, A.M.; Wang, S.; Guiberti, T.F.; Roberts, W.L. Review on the recent advances on ammonia combustion from the fundamentals to the applications. *Fuel Commun.* **2022**, *10*, 100053. [CrossRef]

42. Kurien, C.; Varma, P.S.; Mittal, M. Effect of ammonia energy fractions on combustion stability and engine characteristics of gaseous (ammonia/methane) fuelled spark ignition engine. *Int. J. Hydrogen Energy* **2023**, *48*, 1391–1400. [CrossRef]

43. Huang, F.; Guo, S.; Wang, L.; Yang, Z.; Kong, W. Experimental and numerical study on the performances of a free-piston engine generator using ammonia and methane fuel mixtures. *Fuel* **2023**, *341*, 127654. [CrossRef]

44. Oh, S.; Park, C.; Ahn, M.; Jang, H.J.; Kim, S. Experimental approach for reducing nitrogen oxides emissions from ammonia–natural gas dual-fuel spark-ignition engine. *Fuel* **2023**, *332*, 126065. [CrossRef]

45. Oh, S.; Park, C.; Kim, S.; Kim, Y.; Choi, Y.; Kim, C. Natural gas–ammonia dual-fuel combustion in spark-ignited engine with various air–fuel ratios and split ratios of ammonia under part load condition. *Fuel* **2021**, *290*, 120095. [CrossRef]

46. Mørch, C.S.; Bjerre, A.; Gøttrup, M.P.; Sorenson, S.C.; Schramm, J. Ammonia/hydrogen mixtures in an SI-engine: Engine performance and analysis of a proposed fuel system. *Fuel* **2011**, *90*, 854–864. [CrossRef]

47. Zhang, J.; Luong, M.B.; Im, H.G. Detonation peninsula of different stoichiometric ammonia/hydrogen/air mixtures under engine-relevant conditions. *Combust. Flame* **2023**, *253*, 112793. [CrossRef]

48. Li, J.; Zhang, R.; Pan, J.; Wei, H.; Shu, G.; Chen, L. Ammonia and hydrogen blending effects on combustion stabilities in optical SI engines. *Energy Convers. Manag.* **2023**, *280*, 116827. [CrossRef]

49. Frigo, S.; Gentili, R. Analysis of the behaviour of a 4-stroke Si engine fuelled with ammonia and hydrogen. *Int. J. Hydrogen Energy* **2013**, *38*, 1607–1615. [CrossRef]

50. Xin, G.; Ji, C.; Wang, S.; Hong, C.; Meng, H.; Yang, J. Experimental study on the effect of hydrogen substitution rate on combustion and emission characteristics of ammonia internal combustion engine under different excess air ratio. *Fuel* **2023**, *343*, 127992. [CrossRef]

51. Lhuillier, C.; Brequigny, P.; Contino, F.; Mounaïm-Rousselle, C. Experimental study on ammonia/hydrogen/air combustion in spark ignition engine conditions. *Fuel* **2020**, *269*, 117448. [CrossRef]

52. Lhuillier, C.; Brequigny, P.; Contino, F.; Mounaïm-Rousselle, C. Experimental investigation on ammonia combustion behavior in a spark-ignition engine by means of laminar and turbulent expanding flames. *Proc. Combust. Inst.* **2021**, *38*, 6671–6678. [CrossRef]

53. Dinesh, M.H.; Pandey, J.K.; Kumar, G.N. Study of performance, combustion, and NOₓ emission behavior of an SI engine fuelled with ammonia/hydrogen blends at various compression ratio. *Int. J. Hydrogen Energy* **2022**, *47*, 25391–25403. [CrossRef]

54. Elumalai, R.; Ravi, K. Strategy to reduce carbon emissions by adopting ammonia—Algal biodiesel in RCCI engine and optimize the fuel concoction using RSM methodology. *Int. J. Hydrogen Energy* **2022**, *47*, 39701–39718. [CrossRef]

55. Chen, Y.; Zhang, B.; Su, Y.; Sui, C.; Zhang, J. Effect and mechanism of combustion enhancement and emission reduction for non-premixed pure ammonia combustion based on fuel preheating. *Fuel* **2022**, *308*, 9–11. [CrossRef]

56. Ryu, K.; Zacharakis-Jutz, G.E.; Kong, S.C. Effects of gaseous ammonia direct injection on performance characteristics of a spark-ignition engine. *Appl. Energy* **2014**, *116*, 206–215. [CrossRef]

57. Pandey, J.K.; Dinesh, M.H.; Kumar, G.N. A comparative study of NO_x mitigating techniques EGR and spark delay on combustion and NO_x emission of ammonia/hydrogen and hydrogen fuelled SI engine. *Energy* **2023**, *276*, 127611. [CrossRef]

58. Xin, G.; Ji, C.; Wang, S.; Hong, C.; Meng, H.; Yang, J.; Su, F. Experimental study of the effect of variable valve timing on hydrogen-enriched ammonia engine. *Fuel* **2023**, *344*, 128131. [CrossRef]

59. Xin, G.; Ji, C.; Wang, S.; Hong, C.; Meng, H.; Yang, J.; Su, F. Experimental study on the load control strategy of ammonia-hydrogen dual-fuel internal combustion engine for hybrid power system. *Fuel* **2023**, *347*, 128396. [CrossRef]

60. Hong, C.; Ji, C.; Wang, S.; Xin, G.; Wang, Z.; Meng, H.; Yang, J. An experimental study of various load control strategies for an ammonia/hydrogen dual-fuel engine with the Miller cycle. *Fuel Process. Technol.* **2023**, *247*, 107780. [CrossRef]

61. Wang, B.; Yang, C.; Wang, H.; Hu, D.; Duan, B.; Wang, Y. Study on injection strategy of ammonia/hydrogen dual fuel engine under different compression ratios. *Fuel* **2023**, *334*, 126666. [CrossRef]

62. Pham, Q.; Park, S.; Agarwal, A.K.; Park, S. Review of dual-fuel combustion in the compression-ignition engine: Spray, combustion, and emission. *Energy* **2022**, *250*, 123778. [CrossRef]

63. Kurien, C.; Mittal, M. Utilization of green ammonia as a hydrogen energy carrier for decarbonization in spark ignition engines. *Int. J. Hydrogen Energy* **2023**, *48*, 28803–28823. [CrossRef]

64. Zhang, H.; Li, G.; Long, Y.; Zhang, Z.; Wei, W.; Zhou, M.; Belal, B.Y. Numerical study on combustion and emission characteristics of a spark-ignition ammonia engine added with hydrogen-rich gas from exhaust-fuel reforming. *Fuel* **2023**, *332*, 125939. [CrossRef]

65. Raptotasios, S.I.; Sakellaridis, N.F.; Papagiannakis, R.G.; Hountalas, D.T. Application of a multi-zone combustion model to investigate the NO_x reduction potential of two-stroke marine diesel engines using EGR. *Appl. Energy* **2015**, *157*, 814–823. [CrossRef]

66. Ivanič, Ž.; Ayala, F.; Goldwitz, J.; Heywood, J.B. *Effects of Hydrogen Enhancement on Efficiency and NO_x Emissions of Lean and EGR-Diluted Mixtures in a SI Engine*; SAE Technical Paper; SAE International: Warrendale, PA, USA, 2005. [CrossRef]

67. Dhyani, V.; Subramanian, K.A. Control of backfire and NO_x emission reduction in a hydrogen fueled multi-cylinder spark ignition engine using cooled EGR and water injection strategies. *Int. J. Hydrogen Energy* **2019**, *44*, 6287–6298. [CrossRef]

68. Ezzat, M.F.; Dincer, I. Development and assessment of a new hybrid vehicle with ammonia and hydrogen. *Appl. Energy* **2018**, *219*, 226–239. [CrossRef]

69. Uddeen, K.; Tang, Q.; Shi, H.; Magnotti, G.; Turner, J. A novel multiple spark ignition strategy to achieve pure ammonia combustion in an optical spark-ignition engine. *Fuel* **2023**, *349*, 128741. [CrossRef]

70. Liu, Z.; Zhou, L.; Wei, H. Experimental investigation on the performance of ammonia engine based on reactivity controlled turbulent jet ignition. *Fuel* **2023**, *335*, 127116. [CrossRef]

71. Koike, M.; Suzuoki, T.; Takeuchi, T.; Homma, T.; Hariu, S.; Takeuchi, Y. Cold-start performance of an ammonia-fueled spark ignition engine with an on-board fuel reformer. *Int. J. Hydrogen Energy* **2021**, *46*, 25689–25698. [CrossRef]

72. Ryu, K.; Zacharakis-Jutz, G.E.; Kong, S.C. Performance enhancement of ammonia-fueled engine by using dissociation catalyst for hydrogen generation. *Int. J. Hydrogen Energy* **2014**, *39*, 2390–2398. [CrossRef]

73. Comotti, M.; Frigo, S. Hydrogen generation system for ammonia-hydrogen fuelled internal combustion engines. *Int. J. Hydrogen Energy* **2015**, *40*, 10673–10686. [CrossRef]

74. Oh, S.; Park, C.; Oh, J.; Kim, S.; Kim, Y.; Choi, Y.; Kim, C. Combustion, emissions, and performance of natural gas–ammonia dual-fuel spark-ignited engine at full-load condition. *Energy* **2022**, *258*, 124837. [CrossRef]

75. Bermúdez, V.; Ruiz, S.; Sanchis, E.J.; Conde, B. Assessment of exhaust raw emissions and aftertreatment performance in a retrofitted heavy duty-spark ignition engine operating with liquefied petroleum gas. *J. Clean. Prod.* **2024**, *434*, 140139. [CrossRef]

76. Prikhodko, V.Y.; Pihl, J.A.; Toops, T.J.; Thomas, C.R.; Parks, J.E. Effects of including a NO_x storage component on a TWC when using a lean spark ignition gasoline engine combined with a passive SCR system. *Appl. Energy Combust. Sci.* **2023**, *14*, 100150. [CrossRef]

77. Gainey, B.; Gohn, J.; Hariharan, D.; Rahimi-Boldaji, M.; Lawler, B. Assessing the impact of injector included angle and piston geometry on thermally stratified compression ignition with wet ethanol. *Appl. Energy* **2020**, *262*, 114528. [CrossRef]

78. Xu, L.; Treacy, M.; Zhang, Y.; Aziz, A.; Tuner, M.; Bai, X.S. Comparison of efficiency and emission characteristics in a direct-injection compression ignition engine fuelled with iso-octane and methanol under low temperature combustion conditions. *Appl. Energy* **2022**, *312*, 118714. [CrossRef]

79. Dimitriou, P.; Javaid, R. A review of ammonia as a compression ignition engine fuel. *Int. J. Hydrogen Energy* **2020**, *45*, 7098–7118. [CrossRef]

80. Sun, W.; Zeng, W.; Guo, L.; Zhang, H.; Yan, Y.; Lin, S.; Zhu, G.; Jiang, M.; Yu, C.; Wu, F. An optical study of the combustion and flame development of ammonia-diesel dual-fuel engine based on flame chemiluminescence. *Fuel* **2023**, *349*, 128507. [CrossRef]

81. Lu, Z.; Ye, J.; Gui, Y.; Lu, T.; Shi, L.; An, Y.; Wang, T. Numerical study of the compression ignition of ammonia in a two-stroke marine engine by using HTCGR strategy. *Energy* **2023**, *276*, 127578. [CrossRef]

82. Yousefi, A.; Guo, H.; Dev, S.; Lafrance, S.; Liko, B. A study on split diesel injection on thermal efficiency and emissions of an ammonia/diesel dual-fuel engine. *Fuel* **2022**, *316*, 123412. [CrossRef]

83. Liu, L.; Wu, Y.; Wang, Y. Numerical investigation on the combustion and emission characteristics of ammonia in a low-speed two-stroke marine engine. *Fuel* **2022**, *314*, 122727. [CrossRef]

84. Reiter, A.J.; Kong, S.C. Combustion and emissions characteristics of compression-ignition engine using dual ammonia-diesel fuel. *Fuel* **2011**, *90*, 87–97. [CrossRef]

85. Yousefi, A.; Guo, H.; Dev, S.; Liko, B.; Lafrance, S. Effects of ammonia energy fraction and diesel injection timing on combustion and emissions of an ammonia/diesel dual-fuel engine. *Fuel* **2022**, *314*, 122723. [CrossRef]

86. Zhang, Z.; Long, W.; Dong, P.; Tian, H.; Tian, J.; Li, B.; Wang, Y. Performance characteristics of a two-stroke low speed engine applying ammonia/diesel dual direct injection strategy. *Fuel* **2023**, *332*, 126086. [CrossRef]

87. Liu, L.; Wu, Y.; Wang, Y.; Wu, J.; Fu, S. Exploration of environmentally friendly marine power technology—Ammonia/diesel stratified injection. *J. Clean. Prod.* **2022**, *380*, 135014. [CrossRef]

88. Zhou, X.; Li, T.; Wang, N.; Wang, X.; Chen, R.; Li, S. Pilot diesel-ignited ammonia dual fuel low-speed marine engines: A comparative analysis of ammonia premixed and high-pressure spray combustion modes with CFD simulation. *Renew. Sustain. Energy Rev.* **2023**, *173*, 113108. [CrossRef]

89. Zhu, J.; Zhou, D.; Yang, W.; Qian, Y.; Mao, Y.; Lu, X. Investigation on the potential of using carbon-free ammonia in large two-stroke marine engines by dual-fuel combustion strategy. *Energy* **2023**, *263*, 125748. [CrossRef]

90. Frost, J.; Tall, A.; Sheriff, A.M.; Schönborn, A.; Hellier, P. An experimental and modelling study of dual fuel aqueous ammonia and diesel combustion in a single cylinder compression ignition engine. *Int. J. Hydrogen Energy* **2021**, *46*, 35495–35510. [CrossRef]

91. Al-Dawody, M.F.; Al-Obaidi, W.; Aboud, E.D.; Abdulwahid, M.A.; Al-Farhany, K.; Jamshed, W.; Eid, M.R.; Raizah, Z.; Iqbal, A. Mechanical engineering advantages of a dual fuel diesel engine powered by diesel and aqueous ammonia blends. *Fuel* **2023**, *346*, 128398. [CrossRef]

92. Kuta, K.; Przybyła, G.; Kurzydym, D.; Żmudka, Z. Experimental and numerical investigation of dual-fuel CI ammonia engine emissions and after-treatment with V_2O_5/SiO_2–TiO_2 SCR. *Fuel* **2023**, *334*, 126523. [CrossRef]

93. Şahin, Z.; Ziya Akcanca, İ.; Durgun, O. Experimental investigation of the effects of ammonia solution (NH_3OH) on engine performance and exhaust emissions of a small diesel engine. *Fuel* **2018**, *214*, 330–341. [CrossRef]

94. Lamas, M.I.; Rodriguez, C.G. Numerical model to analyze NO_x reduction by ammonia injection in diesel-hydrogen engines. *Int. J. Hydrogen Energy* **2017**, *42*, 26132–26141. [CrossRef]

95. Jin, Y.; Li, X.; Wang, X.; Ma, Z.; Chu, X. Effect of dimethyl ether on ignition characteristics of ammonia and chemical kinetics. *Fuel* **2023**, *343*, 127885. [CrossRef]

96. Ryu, K.; Zacharakis-Jutz, G.E.; Kong, S.C. Performance characteristics of compression-ignition engine using high concentration of ammonia mixed with dimethyl ether. *Appl. Energy* **2014**, *113*, 488–499. [CrossRef]

97. Pochet, M.; Jeanmart, H.; Contino, F. A 22:1 Compression Ratio Ammonia-Hydrogen HCCI Engine: Combustion, Load, and Emission Performances. *Front. Mech. Eng.* **2020**, *6*, 43. [CrossRef]

98. Pochet, M.; Truedsson, I.; Foucher, F.; Contino, F.; Brussel, V.U. *Ammonia-Hydrogen Blends in Homogeneous-Charge Compression-Ignition Engine*; SAE Technical Paper No. 2017-24-0087; SAE International: Warrendale, PA, USA, 2017. [CrossRef]

99. Wang, H.; Wang, B.; Yang, C.; Hu, D.; Duan, B.; Wang, Y. Study on dual injection strategy of diesel ignition ammonia/hydrogen mixture fuel engine. *Fuel* **2023**, *348*, 128526. [CrossRef]

100. Wang, B.; Wang, H.; Duan, B.; Yang, C.; Hu, D.; Wang, Y. Effect of ammonia/hydrogen mixture ratio on engine combustion and emission performance at different inlet temperatures. *Energy* **2023**, *272*, 127110. [CrossRef]

101. Wang, B.; Yang, C.; Wang, H.; Hu, D.; Wang, Y. Effect of Diesel-Ignited Ammonia/Hydrogen mixture fuel combustion on engine combustion and emission performance. *Fuel* **2023**, *331*, 125865. [CrossRef]

102. Chiong, M.-C.; Chong, C.T.; Ng, J.-H.; Mashruk, S.; Chong, W.W.F.; Samiran, N.A.; Mong, G.R.; Valera-Medina, A. Advancements of combustion technologies in the ammonia-fuelled engines. *Energy Convers. Manag.* **2021**, *244*, 114460. [CrossRef]

103. Gill, S.S.; Chatha, G.S.; Tsolakis, A.; Golunski, S.E.; York, A.P.E. Assessing the effects of partially decarbonising a diesel engine by co-fuelling with dissociated ammonia. *Int. J. Hydrogen Energy* **2012**, *37*, 6074–6083. [CrossRef]

104. Arcoumanis, C.; Bae, C.; Crookes, R.; Kinoshita, E. The potential of di-methyl ether (DME) as an alternative fuel for compression-ignition engines: A review. *Fuel* **2008**, *87*, 1014–1030. [CrossRef]

105. Chen, Z.; Qin, X.; Ju, Y.; Zhao, Z.; Chaos, M.; Dryer, F.L. High temperature ignition and combustion enhancement by dimethyl ether addition to methane-air mixtures. *Proc. Combust. Inst.* **2007**, *31*, 1215–1222. [CrossRef]

106. Gross, C.W.; Kong, S.C. Performance characteristics of a compression-ignition engine using direct-injection ammonia-DME mixtures. *Fuel* **2013**, *103*, 1069–1079. [CrossRef]

107. Bro, K.; Pedersen, P.S. *Alternative Diesel Engine Fuels: An Experimental Investigation of Methanol, Ethanol, Methane and Ammonia in a D.I. Diesel Engine with Pilot Injection*; SAE Technical Paper; SAE International: Warrendale, PA, USA, 1977. [CrossRef]

108. Wang, Y.; Zhou, X.; Liu, L. Feasibility study of hydrogen jet flame ignition of ammonia fuel in marine low speed engine. *Int. J. Hydrogen Energy* **2023**, *48*, 327–336. [CrossRef]

109. Spiteri, A.; Eggenschwiler, P.D.; Liao, Y.; Wigley, G.; Michalow-Mauke, K.A.; Elsener, M.; Kröcher, O.; Boulouchos, K. Comparative analysis on the performance of pressure and air-assisted urea injection for selective catalytic reduction of NO_x. *Fuel* **2015**, *161*, 269–277. [CrossRef]

110. Khristamto Aditya Wardana, M.; Lim, O. Investigation of ammonia homogenization and NO$_x$ reduction quantity by remodeling urea injector shapes in heavy-duty diesel engines. *Appl. Energy* **2022**, *323*, 119586. [CrossRef]

111. Sung, Y.; Choi, M.; Park, T.; Choi, C.; Park, Y.; Choi, G. Synergistic effect of mixer and mixing chamber on flow mixing and NO$_x$ reduction in a marine urea-SCR system. *Chem. Eng. Process. Process Intensif.* **2020**, *150*, 107888. [CrossRef]

112. Ko, A.; Woo, Y.; Jang, J.Y.; Jung, Y.; Pyo, Y.D.; Jo, H.; Lim, O.; Lee, Y.J. Availability of NH$_3$ adsorption in vanadium-based SCR for reducing NO$_x$ emission and NH$_3$ slip. *J. Ind. Eng. Chem.* **2019**, *78*, 433–439. [CrossRef]

113. Kurata, O.; Iki, N.; Inoue, T.; Matsunuma, T.; Tsujimura, T.; Furutani, H.; Kawano, M.; Arai, K.; Okafor, E.C.; Hayakawa, A.; et al. Development of a wide range-operable, rich-lean low-NO$_x$ combustor for NH$_3$ fuel gas-turbine power generation. *Proc. Combust. Inst.* **2019**, *37*, 4587–4595. [CrossRef]

114. Verkamp, F.J.; Hardin, M.C.; Williams, J.R. Ammonia combustion properties and performance in gas-turbine burners. *Symp. Combust.* **1967**, *11*, 985–992. [CrossRef]

115. Li, S.; Li, T.; Wang, N.; Zhou, X.; Chen, R.; Yi, P. An investigation on near-field and far-field characteristics of superheated ammonia spray. *Fuel* **2022**, *324*, 124683. [CrossRef]

116. An, Z.; Xing, J.; Kurose, R. Numerical study on the phase change and spray characteristics of liquid ammonia flash spray. *Fuel* **2023**, *345*, 128229. [CrossRef]

117. Kurata, O.; Iki, N.; Matsunuma, T.; Inoue, T.; Tsujimura, T.; Furutani, H.; Kobayashi, H.; Hayakawa, A. Performances and emission characteristics of NH$_3$-air and NH$_3$-CH$_4$-air combustion gas-turbine power generations. *Proc. Combust. Inst.* **2017**, *36*, 3351–3359. [CrossRef]

118. Zhang, M.; Wei, X.; Wang, J.; Huang, Z.; Tan, H. The blow-off and transient characteristics of co-firing ammonia/methane fuels in a swirl combustor. *Proc. Combust. Inst.* **2021**, *38*, 5859–5868. [CrossRef]

119. Somarathne, K.D.K.A.; Okafor, E.C.; Hayakawa, A.; Kudo, T.; Kurata, O.; Iki, N.; Kobayashi, H. Emission characteristics of turbulent non-premixed ammonia/air and methane/air swirl flames through a rich-lean combustor under various wall thermal boundary conditions at high pressure. *Combust. Flame* **2019**, *210*, 247–261. [CrossRef]

120. Okafor, E.C.; Kurata, O.; Yamashita, H.; Inoue, T.; Tsujimura, T.; Iki, N.; Hayakawa, A.; Ito, S.; Uchida, M.; Kobayashi, H. Liquid ammonia spray combustion in two-stage micro gas turbine combustors at 0.25 MPa; Relevance of combustion enhancement to flame stability and NO$_x$ control. *Appl. Energy Combust. Sci.* **2021**, *7*, 100038. [CrossRef]

121. Okafor, E.C.; Yamashita, H.; Hayakawa, A.; Somarathne, K.K.A.; Kudo, T.; Tsujimura, T.; Uchida, M.; Ito, S.; Kobayashi, H. Flame stability and emissions characteristics of liquid ammonia spray co-fired with methane in a single stage swirl combustor. *Fuel* **2021**, *287*, 119433. [CrossRef]

122. Somarathne, K.D.K.A.; Hatakeyama, S.; Hayakawa, A.; Kobayashi, H. Numerical study of a low emission gas turbine like combustor for turbulent ammonia/air premixed swirl flames with a secondary air injection at high pressure. *Int. J. Hydrogen Energy* **2017**, *42*, 27388–27399. [CrossRef]

123. Zhang, M.; An, Z.; Wang, L.; Wei, X.; Jianayihan, B.; Wang, J.; Huang, Z.; Tan, H. The regulation effect of methane and hydrogen on the emission characteristics of ammonia/air combustion in a model combustor. *Int. J. Hydrogen Energy* **2021**, *46*, 21013–21025. [CrossRef]

124. Viswamithra, V.; Gurunadhan, M.; Menon, S. Expanding swirl combustor operability on methane-ammonia-air mixtures using a distributed fuel injection technique and inlet air preheating. *Int. J. Hydrogen Energy* **2023**, *48*, 1189–1201. [CrossRef]

125. Mikulčić, H.; Baleta, J.; Wang, X.; Wang, J.; Qi, F.; Wang, F. Numerical simulation of ammonia/methane/air combustion using reduced chemical kinetics models. *Int. J. Hydrogen Energy* **2021**, *46*, 23548–23563. [CrossRef]

126. Khateeb, A.A.; Guiberti, T.F.; Zhu, X.; Younes, M.; Jamal, A.; Roberts, W.L. Stability limits and NO emissions of technically-premixed ammonia-hydrogen-nitrogen-air swirl flames. *Int. J. Hydrogen Energy* **2020**, *45*, 22008–22018. [CrossRef]

127. Wei, X.; Zhang, M.; Wang, J.; Huang, Z. Investigation on lean blow-off characteristics and stabilization mechanism of premixed hydrogen enhanced ammonia/air swirl flames in a gas turbine combustor. *Combust. Flame* **2023**, *249*, 112600. [CrossRef]

128. Valera-Medina, A.; Gutesa, M.; Xiao, H.; Pugh, D.; Giles, A.; Goktepe, B.; Marsh, R.; Bowen, P. Premixed ammonia/hydrogen swirl combustion under rich fuel conditions for gas turbines operation. *Int. J. Hydrogen Energy* **2019**, *44*, 8615–8626. [CrossRef]

129. Okafor, E.C.; Somarathne, K.K.A.; Hayakawa, A.; Kudo, T.; Kurata, O.; Iki, N.; Kobayashi, H. Towards the development of an efficient low-NO$_x$ ammonia combustor for a micro gas turbine. *Proc. Combust. Inst.* **2019**, *37*, 4597–4606. [CrossRef]

130. Guteša Božo, M.; Mashruk, S.; Zitouni, S.; Valera-Medina, A. Humidified ammonia/hydrogen RQL combustion in a trigeneration gas turbine cycle. *Energy Convers. Manag.* **2021**, *227*, 113625. [CrossRef]

131. Li, S.; Zhang, S.; Zhou, H.; Ren, Z. Analysis of air-staged combustion of NH$_3$/CH$_4$ mixture with low NO$_x$ emission at gas turbine conditions in model combustors. *Fuel* **2019**, *237*, 50–59. [CrossRef]

132. Xiao, H.; Valera-Medina, A.; Marsh, R.; Bowen, P.J. Numerical study assessing various ammonia/methane reaction models for use under gas turbine conditions. *Fuel* **2017**, *196*, 344–351. [CrossRef]

133. Ariemma, G.B.; Sorrentino, G.; Ragucci, R.; de Joannon, M.; Sabia, P. Ammonia/Methane combustion: Stability and NO$_x$ emissions. *Combust. Flame* **2022**, *241*, 112071. [CrossRef]

134. Wu, Z.; Lv, J.; Liu, X.; Wu, W.; Zhou, S.; Yan, B.; Chen, G. Adiabatic laminar burning velocities and NO generation paths of NH$_3$/H$_2$ premixed flames. *J. Energy Inst.* **2023**, *108*, 101225. [CrossRef]

135. Guteša Božo, M.; Vigueras-Zuniga, M.O.; Buffi, M.; Seljak, T.; Valera-Medina, A. Fuel rich ammonia-hydrogen injection for humidified gas turbines. *Appl. Energy* **2019**, *251*. [CrossRef]

136. Okafor, E.C.; Somarathne, K.K.A.; Ratthanan, R.; Hayakawa, A.; Kudo, T.; Kurata, O.; Iki, N.; Tsujimura, T.; Furutani, H.; Kobayashi, H. Control of NO_x and other emissions in micro gas turbine combustors fuelled with mixtures of methane and ammonia. *Combust. Flame* **2020**, *211*, 406–416. [CrossRef]

137. Cai, Z.; Huang, M.; Wei, G.; Liu, Z.; Fang, H.; Song, Y.; Zhang, M.; Wang, W.; Ming, Z.; Wang, J.; et al. Numerical study of the effect of pressure on the combustion characteristics of ammonia/coal-derived syngas mixture under gas turbine operating conditions. *Fuel* **2023**, *347*, 128463. [CrossRef]

138. Somarathne, K.D.K.A.; Okafor, E.C.; Sugawara, D.; Hayakawa, A.; Kobayashi, H. Effects of OH concentration and temperature on NO emission characteristics of turbulent non-premixed $CH_4/NH_3/air$ flames in a two-stage gas turbine like combustor at high pressure. *Proc. Combust. Inst.* **2021**, *38*, 5163–5170. [CrossRef]

139. Tang, Y.; Xie, D.; Shi, B.; Wang, N.; Li, S. Flammability enhancement of swirling ammonia/air combustion using AC powered gliding arc discharges. *Fuel* **2022**, *313*, 122674. [CrossRef]

140. Vijrumbana, Y.; Singh, A.S.; Vakamalla, T.R.; Mahendra Reddy, V. A chemical kinetic analysis: Influence of post-flame chemistry, combustion pressure, premixing degree (fully premixed to non-premixed), and secondary air supply on NO_x emissions from NH3/CH4-air combustion. *Therm. Sci. Eng. Prog.* **2023**, *40*, 101750. [CrossRef]

141. Shahsavari, M.; Konnov, A.A.; Bai, X.S.; Valera-Medina, A.; Li, T.; Jangi, M. Synergistic effects of nanosecond plasma discharge and hydrogen on ammonia combustion. *Fuel* **2023**, *348*, 128475. [CrossRef]

142. Belal, B.Y.; Li, G.; Zhang, Z.; El-Batsh, H.M.; Moneib, H.A.; Attia, A.M.A. The effect of swirl burner design configuration on combustion and emission characteristics of lean pre-vaporized premixed flames. *Energy* **2021**, *228*, 120622. [CrossRef]

143. Mashruk, S.; Okafor, E.; Kovaleva, M.; Alnasif, A.; Pugh, D.; Hayakawa, A.; Valera-Medina, A. Evolution of N_2O production at lean combustion condition in $NH_3/H_2/air$ premixed swirling flames. *Combust. Flame* **2022**, *244*, 112299. [CrossRef]

144. Ouyang, W.; Zheng, S.; Wu, C.; Hu, X.; Chen, R.; Zhuo, L.; Wang, Z. Dynamic ammonia adsorption by FAU zeolites to below 0.1 ppm for hydrogen energy applications. *Int. J. Hydrogen Energy* **2021**, *46*, 32559–32569. [CrossRef]

145. Dincer, I.; Siddiqui, O. Types of fuels. In *Ammonia Fuel Cells*; Elsevier: Amsterdam, The Netherlands, 2020. [CrossRef]

146. Dincer, I.; Siddiqui, O. Ammonia fuel cells. In *Ammonia Fuel Cells*; Elsevier: Amsterdam, The Netherlands, 2020; Volume 4. [CrossRef]

147. Hu, J.; Liang, Q.; He, X.; Xia, S.; Liu, Y. Bio-inspired design of a fence-type triangular flow channel for ammonia-hydrogen fuel cells. *Int. J. Hydrogen Energy* **2023**, *52*, 799–815. [CrossRef]

148. Ye, M.; Sharp, P.; Brandon, N.; Kucernak, A. System-level comparison of ammonia, compressed and liquid hydrogen as fuels for polymer electrolyte fuel cell powered shipping. *Int. J. Hydrogen Energy* **2022**, *47*, 8565–8584. [CrossRef]

149. Zhong, C.; Hu, W.B.; Cheng, Y.F. Recent advances in electrocatalysts for electro-oxidation of ammonia. *J. Mater. Chem. A* **2013**, *1*, 3216–3238. [CrossRef]

150. El-Shafie, M.; Kambara, S.; Hayakawa, Y. Development of zeolite-based catalyst for enhancement hydrogen production from ammonia decomposition. *Catal. Today* **2022**, *397–399*, 103–112. [CrossRef]

151. Wang, Z.; Zhang, H.; Ye, Z.; He, G.; Liao, C.; Deng, J.; Lei, G.; Zheng, G.; Zhang, K.; Gou, F.; et al. H_2 production from ammonia decomposition with Mo_2N catalyst driven by dielectric barrier discharge plasma. *Int. J. Hydrogen Energy* **2023**, *49*, 1375–1385. [CrossRef]

152. Armenise, S.; Cazaña, F.; Monzón, A.; García-Bordejé, E. In situ generation of CO_x-free H_2 by catalytic ammonia decomposition over Ru-Al-monoliths. *Fuel* **2018**, *233*, 851–859. [CrossRef]

153. Seyfeli, R.C.; Varisli, D. Performance of microwave reactor system in decomposition of ammonia using nickel based catalysts with different supports. *Int. J. Hydrogen Energy* **2022**, *47*, 15175–15188. [CrossRef]

154. Wang, X.; Zhang, Z.; Zhou, G.; Zhang, Y.; Zhao, X.; Han, D.; Chen, T.; Huang, Z.; Lin, H. Synergistic effect between electric field and Ce-doped catalysts to promote hydrogen production from ammonia decomposition. *Fuel* **2023**, *351*, 128796. [CrossRef]

155. Noskov, A.; Zolotarskii, I.; Pokrovskaya, S.; Kashkin, V.; Slavinskaya, E.; Mokrinskii, V.; Korotkikh, V. Ammonia oxidation into nitrous oxide over Mn/Bi/Al catalyst: II. Fluidized bed reactor experiments. *Chem. Eng. J.* **2005**, *107*, 79–87. [CrossRef]

156. Warner, M.; Haynes, B.S. Formation of N_2 and N_2O in industrial combustion of ammonia over platinum. *Proc. Combust. Inst.* **2015**, *35*, 2215–2222. [CrossRef]

157. Chiuta, S.; Everson, R.C.; Neomagus, H.W.J.P.; Bessarabov, D.G. Hydrogen production from ammonia decomposition over a commercial Ru/Al_2O_3 catalyst in a microchannel reactor: Experimental validation and CFD simulation. *Int. J. Hydrogen Energy* **2016**, *41*, 3774–3785. [CrossRef]

158. Vernikovskaya, N.V.; Pinaeva, L.G.; Isupova, L.A. Oxidation of ammonia to NO_x in a two bed reactor (Pt gauzes+oxide monolytic layer): Experimental studies and mathematical modelling. *Chem. Eng. J.* **2014**, *238*, 140–147. [CrossRef]

159. Chiuta, S.; Bessarabov, D.G. Design and operation of an ammonia-fueled microchannel reactor for autothermal hydrogen production. *Catal. Today* **2018**, *310*, 187–194. [CrossRef]

160. He, X.; Liu, Z.; Jiang, H.; Yang, Q.; Jiang, Z.; Feng, G.; Zhao, C. Super adiabatic flame temperature phenomenon for NH3/O2/N2 mixtures. *Fuel* **2023**, *346*, 128264. [CrossRef]

161. Ilbas, M.; Kekul, O.; Bektas, A.; Karyeyen, S. Oxidizer effects on ammonia combustion using a generated non-premixed burner. *Int. J. Hydrogen Energy* **2022**, *47*, 12317–12337. [CrossRef]

162. Yang, W.; Ranga Dinesh, K.K.J.; Luo, K.H.; Thevenin, D. Direct numerical simulation of turbulent premixed ammonia and ammonia-hydrogen combustion under engine-relevant conditions. *Int. J. Hydrogen Energy* **2022**, *47*, 11083–11100. [CrossRef]

163. Scharl, V.; Lackovic, T.; Sattelmayer, T. Characterization of ammonia spray combustion and mixture formation under high-pressure, direct injection conditions. *Fuel* **2023**, *333*, 126454. [CrossRef]

164. Zhu, S.; Xu, Q.; Tang, R.; Gao, J.; Wang, Z.; Pan, J.; Zhang, D. A comparative study of oxidation of pure ammonia and ammonia/dimethyl ether mixtures in a jet-stirred reactor using SVUV-PIMS. *Combust. Flame* **2023**, *250*, 112643. [CrossRef]

165. Ju, R.; Wang, J.; Zhang, M.; Mu, H.; Zhang, G.; Yu, J.; Huang, Z. Stability and emission characteristics of ammonia/air premixed swirling flames with rotating gliding arc discharge plasma. *Energy* **2023**, *277*, 127649. [CrossRef]

166. Vijrumbana, Y.; Shankar Singh, A.; Jik Lee, B.; Mahendra Reddy, V. Chemical kinetic analysis to study the potential of fuel staging in reducing the emissions from NH_3/CH_4-air combustion at different pressures. *Fuel* **2023**, *339*, 127404. [CrossRef]

167. Mashruk, S.; Kovaleva, M.; Alnasif, A.; Chong, C.T.; Hayakawa, A.; Okafor, E.C.; Valera-Medina, A. Nitrogen oxide emissions analyses in ammonia/hydrogen/air premixed swirling flames. *Energy* **2022**, *260*, 125183. [CrossRef]

168. Tomidokoro, T.; Yokomori, T.; Im, H.G. Numerical study on propagation and NO reduction behavior of laminar stratified ammonia/air flames. *Combust. Flame* **2022**, *241*, 112102. [CrossRef]

169. Bykov, V.; Stein, M.; Maas, U. Study of mechanism of ammonia decomposition and oxidation: From NO_x reduction to ammonia auto-ignition problem. *Proc. Combust. Inst.* **2023**, *39*, 4267–4275. [CrossRef]

170. Yu, J.; Jiang, Z.; Hou, M.; Liang, D.; Xiao, Y.; Dou, M.; Shao, Z.; Yi, B. Analysis of the behavior and degradation in proton exchange membrane fuel cells with a dead-ended anode. *J. Power Sources* **2014**, *246*, 90–94. [CrossRef]

171. Siegel, J.B.; Bohac, S.V.; Stefanopoulou, A.G.; Yesilyurt, S. Nitrogen Front Evolution in Purged Polymer Electrolyte Membrane Fuel Cell with Dead-Ended Anode. *J. Electrochem. Soc.* **2010**, *157*, B1081. [CrossRef]

172. Du, Z.; Liu, C.; Zhai, J.; Guo, X.; Xiong, Y.; Su, W.; He, G. A review of hydrogen purification technologies for fuel cell vehicles. *Catalysts* **2021**, *11*, 393. [CrossRef]

173. Lin, L.; Tian, Y.; Su, W.; Luo, Y.; Chen, C.; Jiang, L. Techno-economic analysis and comprehensive optimization of an on-site hydrogen refuelling station system using ammonia: Hybrid hydrogen purification with both high H_2 purity and high recovery. *Sustain. Energy Fuels* **2020**, *4*, 3006–3017. [CrossRef]

174. Patki, N.S.; Lundin, S.T.B.; Way, J.D. Apparent activation energy for hydrogen permeation and its relation to the composition of homogeneous PdAu alloy thin-film membranes. *Sep. Purif. Technol.* **2018**, *191*, 370–374. [CrossRef]

175. Zhang, Z.; Liguori, S.; Fuerst, T.F.; Way, J.D.; Wolden, C.A. Efficient Ammonia Decomposition in a Catalytic Membrane Reactor to Enable Hydrogen Storage and Utilization. *ACS Sustain. Chem. Eng.* **2019**, *7*, 5975–5985. [CrossRef]

176. Cechetto, V.; Struijk, C.L.; Di Felice, L.; de Leeuw den Bouter, A.W.N.; Gallucci, F. Adsorbents development for hydrogen cleanup from ammonia decomposition in a catalytic membrane reactor. *Chem. Eng. J.* **2023**, *455*, 140762. [CrossRef]

177. Cerrillo, J.L.; Morlanés, N.; Kulkarni, S.R.; Realpe, N.; Ramírez, A.; Katikaneni, S.P.; Paglieri, S.N.; Lee, K.; Harale, A.; Solami, B.; et al. High purity, self-sustained, pressurized hydrogen production from ammonia in a catalytic membrane reactor. *Chem. Eng. J.* **2022**, *431*, 134310. [CrossRef]

178. Makhloufi, C.; Kezibri, N. Large-scale decomposition of green ammonia for pure hydrogen production. *Int. J. Hydrogen Energy* **2021**, *46*, 34777–34787. [CrossRef]

179. Zhao, J.F.; Liang, Y.F.; Liang, Q.C.; Li, M.J.; Hu, J.Y. Experimental and Simulation Study of PEMFC based on Ammonia Decomposition Gas as Fuel. *J. Electrochem. Sci. Technol.* **2022**, *13*, 63–70. [CrossRef]

180. Zhao, Y.; Setzler, B.P.; Wang, J.; Nash, J.; Wang, T.; Xu, B.; Yan, Y. An Efficient Direct Ammonia Fuel Cell for Affordable Carbon-Neutral Transportation. *Joule* **2019**, *3*, 2472–2484. [CrossRef]

181. Hu, J.; Liang, Q.; Li, M.; He, X.; Zhao, J.; Liu, Z.; Xia, S. Numerical simulation of gas–heat–water distribution characteristics of Ammonia–Hydrogen fuel cell. *Energy Rep.* **2022**, *8*, 9787–9804. [CrossRef]

182. Hunter, H.M.; Makepeace, J.W.; Wood, T.J.; Mylius, O.S.; Kibble, M.G.; Nutter, J.B.; Jones, M.O.; David, W.I. Demonstrating hydrogen production from ammonia using lithium imide—Powering a small proton exchange membrane fuel cell. *J. Power Sources* **2016**, *329*, 138–147. [CrossRef]

183. Lin, L.; Zhang, L.; Luo, Y.; Luo, J.; Chen, C.; Jiang, L. Highly-integrated and Cost-efficient Ammonia-fueled fuel cell system for efficient power generation: A comprehensive system optimization and Techno-Economic analysis. *Energy Convers. Manag.* **2022**, *251*, 114917. [CrossRef]

184. Zhao, J.; Liang, Q.; Liang, Y.; Hu, J. Experimental and 3D simulation study of a nitrogen-hydrogen fueled PEMFC. *Int. J. Electrochem. Sci.* **2022**, *17*, 220313. [CrossRef]

185. Woo, M.; Choi, B.C. Numerical study on fuel-NO formation characteristics of ammonia-added methane fuel in laminar non-premixed flames with oxygen/carbon dioxide oxidizer. *Energy* **2021**, *226*, 120365. [CrossRef]

186. Cai, T.; Zhao, D.; Wang, B.; Li, J.; Guan, Y. NO_x emission and thermal performances studies on premixed ammonia-oxygen combustion in a CO_2-free micro-planar combustor. *Fuel* **2020**, *280*, 118554. [CrossRef]

187. Ilbas, M.; Alemu, M.A.; Cimen, F.M. Comparative performance analysis of a direct ammonia-fuelled anode supported flat tubular solid oxide fuel cell: A 3D numerical study. *Int. J. Hydrogen Energy* **2022**, *47*, 3416–3428. [CrossRef]

188. Feng, G.; Chen, J.; Fan, W.; Wang, X. Study of the interaction between NH_3 and NO in the reduction zone of air-staged ammonia combustion under high moisture atmosphere. *J. Clean. Prod.* **2023**, *409*, 137218. [CrossRef]

189. Sun, Z.; Xu, J.; Su, S.; Qing, M.; Wang, L.; Cui, X.; Mostafa, M.E.; Zhang, C.; Hu, S.; Wang, Y.; et al. Formation and reduction of NO from the oxidation of NH_3/CH_4 with high concentration of H_2O. *Fuel* **2019**, *247*, 19–25. [CrossRef]

190. Choe, J.; Sun, W.; Ombrello, T.; Carter, C. Plasma assisted ammonia combustion: Simultaneous NO$_x$ reduction and flame enhancement. *Combust. Flame* **2021**, *228*, 430–432. [CrossRef]
191. Wickham, D.T.; Lind, J. *Catalysts for the Selective Oxidation of Ammonia to Nitrogen and Water*; SAE Technical Paper; SAE International: Warrendale, PA, USA, 2003. [CrossRef]
192. Engelbrecht, N.; Chiuta, S.; Bessarabov, D.G. A highly efficient autothermal microchannel reactor for ammonia decomposition: Analysis of hydrogen production in transient and steady-state regimes. *J. Power Sources* **2018**, *386*, 47–55. [CrossRef]
193. Stagni, A.; Cavallotti, C.; Arunthanayothin, S.; Song, Y.; Herbinet, O.; Battin-Leclerc, F.; Faravelli, T. An experimental, theoretical and kinetic-modeling study of the gas-phase oxidation of ammonia. *React. Chem. Eng.* **2020**, *5*, 696–711. [CrossRef]
194. Meng, X.; Zhao, C.; Cui, Z.; Zhang, X.; Zhang, M.; Tian, J.; Long, W.; Bi, M. Understanding of combustion characteristics and NO generation process with pure ammonia in the pre-chamber jet-induced ignition system. *Fuel* **2023**, *331*, 125743. [CrossRef]
195. Wang, Y.; Zhou, X.; Liu, L. Study on the mechanism of the ignition process of ammonia/hydrogen mixture under high-pressure direct-injection engine conditions. *Int. J. Hydrogen Energy* **2021**, *46*, 38871–38886. [CrossRef]